AD-A110 957 SCRIPPS INSTITUTION OF OCEANOGRAPHY LA JOLLA CALIF I--ETC F/G 20/4
REMOTE SYNOPTIC SURFACE FLOW MEASUREMENTS IN SMALL BODIES OF WA--ETC(U)
SEP 80 D SHERES, J D ISAACS N00014-76-C-1103

UNCLASSIFIED NL

1 OF 2
AD A
110957

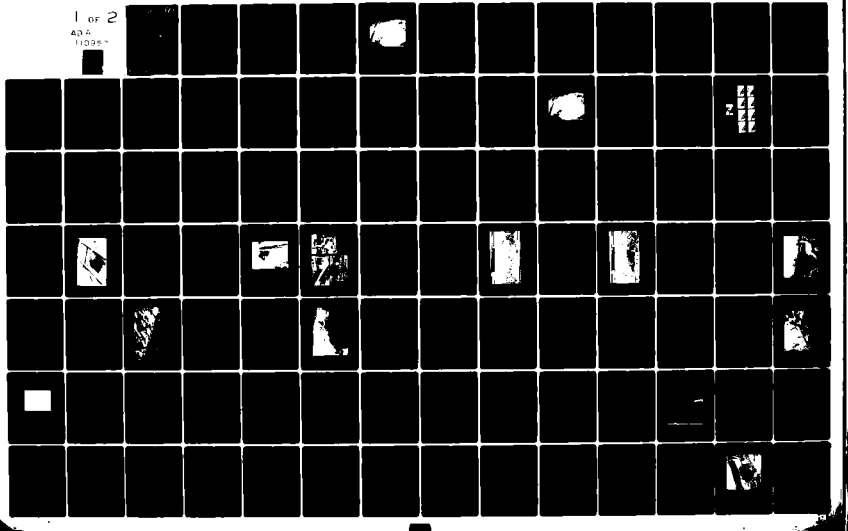

LEVEL II

REMOTE SYNOPTIC SURFACE FLOW MEASUREMENTS IN SMALL BODIES OF WATER

DAVID SHERES

1980

Remote Synoptic Surface Flow Measurements in Small Bodies of Water

Final Report

Contract Number: N00014-76-1103

Office of Naval Research, Geography Program

Principal Investigator: John D.Isaacs

Research Assistant : David Sheres

September 1980

UNCLASSIFIED

SECURITY CLASSIFICATION OF THIS PAGE (When Data Entered)

REPORT DOCUMENTATION PAGE		READ INSTRUCTIONS BEFORE COMPLETING FORM
1. REPORT NUMBER	2. GOVT ACCESSION NO.	3. RECIPIENT'S CATALOG NUMBER
4. TITLE (and Subtitle) REMOTE SYNOPTIC SURFACE FLOW MEASUREMENTS IN SMALL BODIES OF WATER		5. TYPE OF REPORT & PERIOD COVERED FINAL 6. PERFORMING ORG. REPORT NUMBER
7. AUTHOR(s) David Sheres		8. CONTRACT OR GRANT NUMBER(s) N00014-76-C-1103
9. PERFORMING ORGANIZATION NAME AND ADDRESS Scripps Institution of Oceanography Institute of Marine Resources La Jolla, CA 92093		10. PROGRAM ELEMENT, PROJECT, TASK AREA & WORK UNIT NUMBERS
11. CONTROLLING OFFICE NAME AND ADDRESS Office of Naval Research Coastal Sciences Program Arlington, Virginia 22217		12. REPORT DATE (September) 1980 13. NUMBER OF PAGES
14. MONITORING AGENCY NAME & ADDRESS(if different from Controlling Office)		15. SECURITY CLASS. (of this report) Unclassified 15a. DECLASSIFICATION/DOWNGRADING SCHEDULE

16. DISTRIBUTION STATEMENT (of this Report)

Distribution Unlimited.

17. DISTRIBUTION STATEMENT (of the abstract entered in Block 20, if different from Report)

18. SUPPLEMENTARY NOTES

John D. Isaacs was Principal Investigator. A part of this report will be published in the Journal of Physical Oceanography.

19. KEY WORDS (Continue on reverse side if necessary and identify by block number)

Remote Sensing
Current Measurements
Wave Measurements
Wave-Current Interaction
Experimental Facilities for Wave Current Interaction
Optical Processing of Wave Data
Glitter Pattern

20. ABSTRACT (Continue on reverse side if necessary and identify by block number)

This report describes a novel approach to remote and synoptic surface flow measurements in small bodies of water; it also includes an investigation to determine the practicality of this technique. The approach is based on imaging monochromatic wavetrains, of known frequency, propagating over surface flows. The report shows that the wavelength and direction of two monochromatic wave trains of known frequency, at a region of interest, carry all the necessary information to determine (Continued on reverse)

DD FORM 1 JAN 73 1473 EDITION OF 1 NOV 65 IS OBSOLETE
S/N 0102-014-6601

UNCLASSIFIED

SECURITY CLASSIFICATION OF THIS PAGE (When Data Entered)

the surface flow in that region. Experimental tests, conducted both in a wavetank and in a lagoon, utilizing inexpensive and readily available equipment, are described as well. These tests have shown the viability of this remote and synoptic surface flow measurement. Practical aspects of the measurements, such as vertically nonhomogeneous flow profiles, data processing of the aerial photos via 2D Fourier transforms, and the measurement of wavelength by photography of specular reflection of sun light from waves, are discussed as well. The extension of this measurement to coastal regions in the open ocean is briefly explored together with a preliminary experiment that tests the possibility of obtaining quantitative flow data from boat wave measurements. Such utilization of boat waves may enable surface flow measurements in areas otherwise inaccessible.

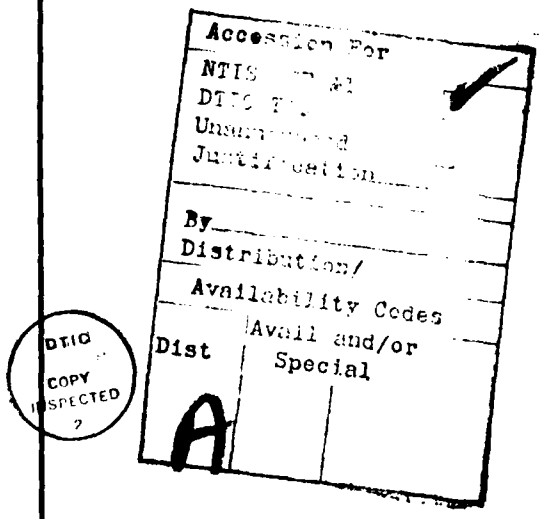

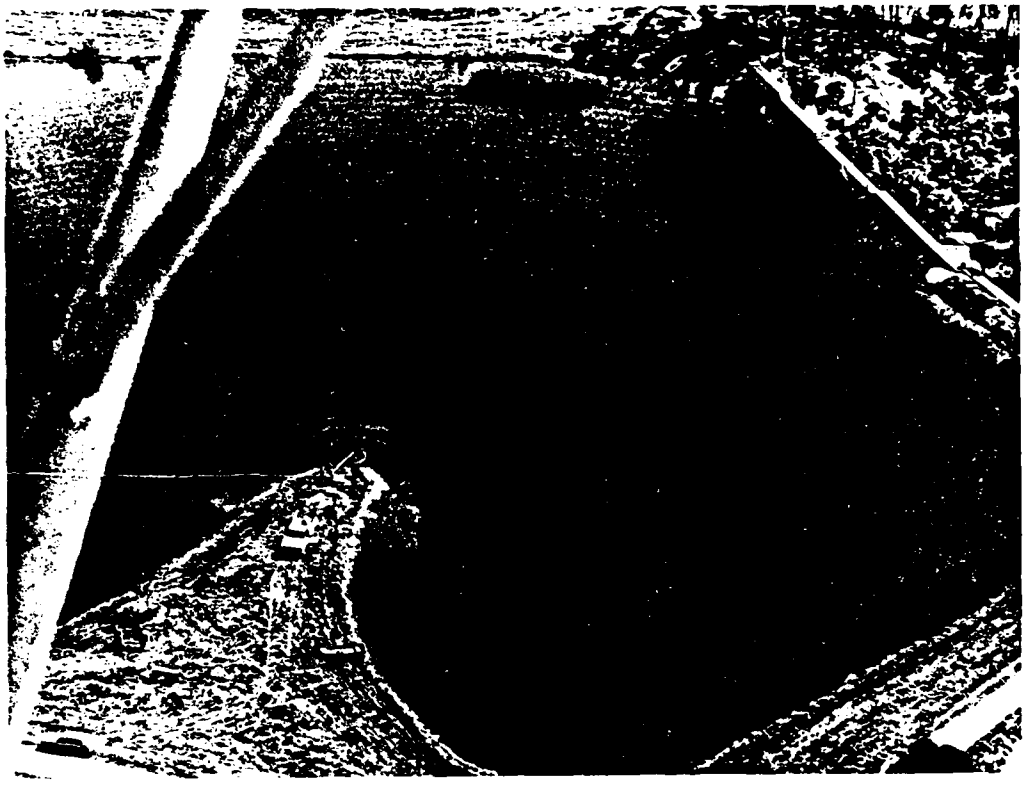

FRONTISPIECE

Illuminating the lake in Rancho Zorro with a one manpower, variable frequency, wave generator.

UNIVERSITY OF CALIFORNIA

San Diego

Remote Synoptic Surface Flow Measurements in Small Bodies of Water

A dissertation submitted in partial satisfaction of the requirements for the degree Doctor of Philosophy in Oceanography

by

David Sheres

Committee in charge:

Professor John D. Isaacs, Chairman

Professor Victor C. Anderson

Mr. James L. Harris, Senior

Professor Myrl C. Henderschott

Professor Joseph L. Reid

1980

The dissertation of David Sheres is approved, and it is acceptable in quality and form for publication on microfilm:

Chairman

University of California, San Diego

1980

To Ita

TABLE OF CONTENTS

List of Symbols

C_o	Wave phase speed in stationary water, measured by a stationary observer.
C	wave phase speed in a flow, measured by an observer moving with the flow.
D	Depth where flow has maximum velocity.
d	Spacing between lines in a grating.
k	Wavenumber
ℓ	Distance in the Fourier plane.
L	Wavelength of waves in a flow.
L_o	Wavelength of waves in stationary water.
T_o	Wave period of waves in stationary water, measured by a stationary observer.
T	Wave period of waves in a flow, measured by an observer moving with the flow.
U	Surface flow speed.
z	Depth.
α_n	Angle between wave crest in stationary water and flow direction (angle of incidence).
α	Angle between wave crest in the flow and flow direction.
λ	Wavelength of light.
σ	Angular frequency.

List of Figures

Page

List of Tables

Acknowledgments

I wish to acknowledge the following people whose help in completing this research was invaluable:

My wife, Ita, who has encouraged me to pursue the projects that I wanted to undertake; her continuous help before and during my tenure at Scripps made this thesis possible.

John Isaacs whose valuable ideas, comments and suggestions helped in this work from its conceptual "birth" to completion; his oceanographic expertise aided in navigating this thesis on a successful course.

John Lyons who was instrumental in every facet of the experimental work: his resourcefulness and enthusiasm were a major contribution to this research.

The staff of the Foundation for Ocean Research, who have always been ready to help any way they could; David Castel, Steve Costa, Dick Schwartzlose, Jim Stork and Gerry Wick were most helpful.

My committee members, who were always positive and encouraging, and helped me "sail" through.

The Foundation for Ocean Research and Office of Naval Research who funded this research, and Edwin Florence, who acted as a constructive Office of Naval Research monitor.

VITA

June 27, 1937 — Born — Tel Aviv, Israel

1962 — B.S., Electrical Engineering, Massachusetts Institute of Technology, Cambridge, Massachusetts

1964 — M.S., Electrical Engineering, University of Wisconsin, Madison

1964-1966 — Marketing, Electrical Equipment Co., Tel Aviv, Israel

1966-1969 — Instructor, Technion, Haifa, Israel

1969-1970 — Project manager, Carson Laboratories, Bristol, Connecticut

1973-1979 — Research Assistant, Scripps Institution of Oceanography University of California, San Diego, and the Foundation for Ocean Research, San Diego, California

PUBLICATIONS

"Remote and Synoptic Water Wave Measurements by Aerial Photography: A Model, Experimental Results and an Application." Proceedings of Ocean '79 Conference, San Diego, CA. pp. 614-622, September 1979.

FIELDS OF STUDY

Major Field: Oceanography

Studies in Physical Oceanography
Professor J. L. Reid

Studies in Dynamical Oceanography
Professor R. S. Arthur

Studies in Waves
Professor M. C. Henderschott

Studies in Fluid Dynamics
Professor C. D. Winant

Studies in Near Shore Processes
Professor D. L. Inman

Studies in Oceanographic Experiments
Professor W. Munk

Studies in General Oceanography
Professor J. D. Isaacs

ABSTRACT OF THE DISSERTATION

Remote Synoptic Surface Flow Measurements
in Small Bodies of Water

by

David Sheres
Doctor of Philosophy in Oceanography
University of California, San Diego, 1980
Professor John D. Isaacs, Chairman

This thesis describes a novel approach to remote and synoptic surface flow measurements in small bodies of water; it also includes an investigation to determine the practicality of this technique. The approach is based on imaging monochromatic wavetrains, of known frequency, propagating over surface flows. The thesis shows that the wavelength and direction of two monochromatic wave trains of known frequency, at a region of interest, carry all the necessary information to determine the surface flow in that region. Experimental tests, conducted both in a wavetank and in a lagoon, utilizing inexpensive and readily available equipment, are described as well. These tests have shown the viability of this remote and synoptic surface flow measurement. Practical aspects of the measurements, such as vertically nonhomogeneous flow profiles, data processing of the aerial photos via

2D Fourier transforms, and the measurement of wavelength by photography of specular reflection of sun light from waves, are discussed as well. The extension of this measurement to coastal regions in the open ocean is briefly explored together with a preliminary experiment that tests the possibility of obtaining quantitative flow data from boat wave measurements. Such utilization of boat waves may enable surface flow measurements in areas otherwise inaccessible.

FRONTISPIECE

Illuminating the lake in Rancho Zorro with a one manpower, variable frequency, wave generator.

Introduction

The challenge

Small-scale circulation in harbors and bays have a direct effect on the transport and accumulation of nutrients, pollutants, sediment, and other suspended and dissolved materials. The interaction between surface currents and waves has a marked effect on the sea state. It is evident that patterns of water circulation influence shoaling, biological activity, and various maritime and recreational activities. Clearly, a simple and inexpensive way of determining the distribution of surface flows, both spatial and temporal, will prove beneficial.

Most measurements of currents (with the exception of radar scattering) either give data at the point where the recorder is stationed, or give a parcel trajectory; the Eulerian versus the Lagrangian approach. In order to ascertain a synoptic current distribution in detail over a sizeable area, a large number of recorders sampling the current at their respective positions or great numbers of tracked drifters are required. Synoptic recording of surface currents would eliminate the multiplicity of recorders or current drogues, the problems of deployment, and cumulative errors associated with analysis. Linear surface waves provide a sensor for such synoptic recording, and the waves' aerial photographs permit current measurements in areas not accessible to conventional approaches.

This thesis offers an investigation, both theoretical and experimental, into the application of wave-current interactions for remote and synoptic surface flow determination.

Related previous work

Unna (1942) described the interaction between waves and a codirectional flow. Johnson (1947) first described quantitatively the interaction between uniform flows and waves at oblique incidence. This treatment was based on the changes in the refracting waves at the flow boundaries. A similar approach to horizontal shear flows was offered by Longuet-Higgins and Stewart (1961). Isaacs (1948) presented observations of qualitative changes of the sea state due to different flow regimes and their influence on navigation, both in the open ocean and at coastal entrances off Oregon and Washington. Figure 1 furnishes successive photos that I took at Scripps' HydroLab of waves propagating into a flat bottom channel, that models an estuary at ebb tide. This is similar to Isaacs' observation of waves converging at the middle of an entrance at ebb tide, causing large slope waves there that are hazardous for navigation. Some unusually large waves, reported in the Indian Ocean near southeast Africa (Kipling, 1893; Schuman, 1975) may be due to such interaction of the Aghulas current with southwesterly swell. Kenyon (1971) calculated the propagation of waves and wave energy due to horizontal shear; he then followed with a discussion of the effects of major ocean currents in refracting and trapping wave energy. In this work I deal with the inverse problem, namely, how can the surface circulation pattern be deduced from a measured wavefield? Huang (1972) *et al.* attempted to do that: they suggested that surface flows could be estimated from wave slope measurements. Their model is one dimensional (the waves and flows are in the same direction), and they assume that the wind generated waves are generated outside the

No channel flow

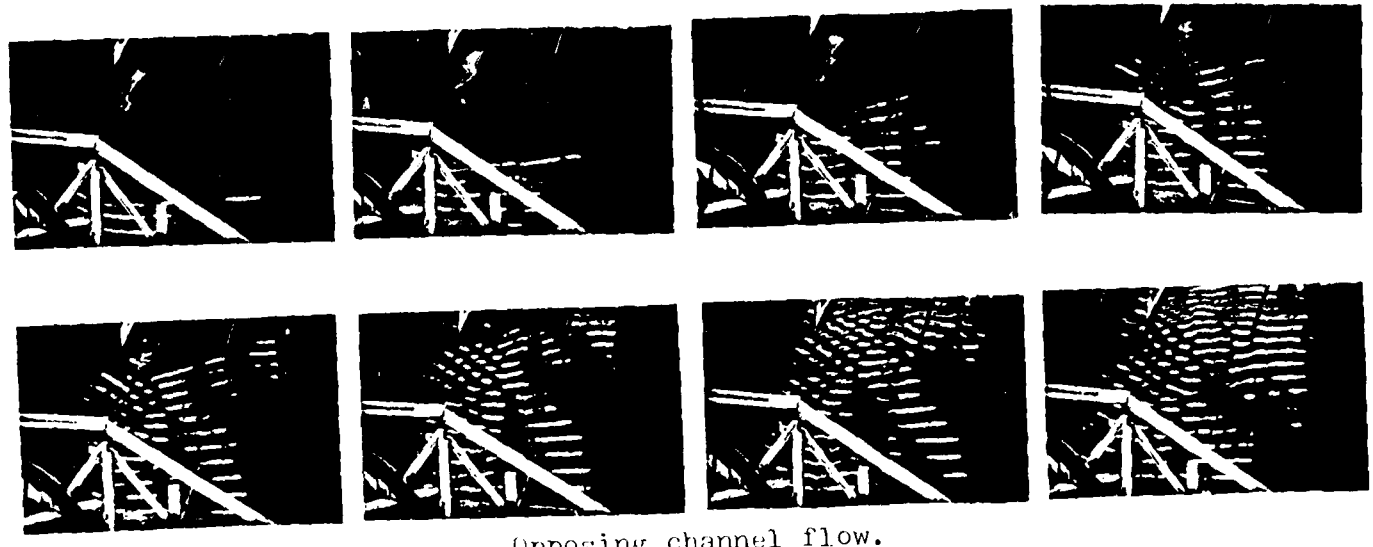

Opposing channel flow.
Photos proceed from left to right.

Figure 1. Waves propagating into a channel. Wave generator in foreground.

flow. There was no mention of experimental exploration of this approach. Sugimori (1973) has taken aerial photos of the surface waves in and nearby to the Kuroshio current. He analyzed these photos for the directional spectrum of the surface waves by optically obtaining their two-dimensional Fourier transforms, in order to correlate the changes in the directional spectrum with the Juroshio flow. The results that he obtained were inconclusive, and one of the reasons for that is, I assume, that he looked at directional spectra for waves with wavelength from .5 to 5 meters. Such waves are relatively slow (.88 to 2.8 m/sec) and would have most likely been totally reflected, or dissipated by breaking, when encountering the flow. Thus the waves he observed inside the Juroshio were mostly generated there, rather than propagated into the flow from nearby stationary waters. A modification of Sugimori's experiment, to analyze the directional spectra of longer waves, could supply more illuminating results. Flying the photographic airplane at higher altitudes than the 450 m used by Sugimori, will aid in obtaining such spectra. The appendix of this thesis considers the effect of altitude in aerial photography of waves, and could help determine the appropriate altitude for such an experiment.

Stewart and Joy (1974) have used resonant doppler scattering of radio waves by a small segment of the ocean's directional spectrum, to measure the surface flow of ocean currents. They compared the speed of the water waves, as measured by the Doppler shift in the scattered radio waves, to the expected water wave speed; the latter was deduced from their wavelength, which is half that of the radio waves. This method assumes a truly continuous wave spectrum directed

radially towards the radar system. Very sensitive measurements are required to obtain data. This method may be useful in remote sensing of large-scale surface flow (the scale is related to the radar pulse width, antenna beam width and spacing between transmitters). Evans and Georges (1979) report on the development of an instrument utilizing resonant doppler scattering to measure nearshore surface currents out to a maximum range of 60 km offshore. They report that a map containing 800 current vectors covering 2000 square kilometers of ocean can be produced automatically in 45 minutes. Thus each current reading is an average of a cell of more than 1 km on the side. They did not state what was the minimum range of their instrument. Their current maps seem inconvincingly regular and precise, which may be imposed by their data processing.

This Research

Surface water waves have the property, lacking in most other wave systems, that they can be easily observed over a relatively large spatial region containing many waves. The wavelength of water waves despends on the surface velocity field (and the bathymetry) in the water over which they propagate, hence the wavelength distribution of waves in a region contains informative data about the surface flow in that region.

In this thesis, I have set out to develop a surface flow

measuring system, based on observations of coherent wave trains at the region of interest. The wave observations, conducted by aerial photography, makes this a remote sensing technique capable of flow determination in non-accessible areas. It is also a synoptic flow measuring system; each point in the aerial image that shows coherent wave trains (of known frequency), also carries information concerning the speed and direction of the surface flow there.

The approach described here is based on two factors: first, that the wave length of a train of coherent waves in the flow has the same value both when observed by a stationary observer and by an observer moving with the flow. Second, that the period of a wave train measured by a stationary observer, has the same value whether the wave train is in stationary or flowing water. This is a consequence of conservation of the number of wave crests, and holds for flow patterns that are stationary or slowly varying with time. Herbich and Hale (1972) have confirmed experimentally the invariance of T_o. (This period, T_o, is, of course, different than the period measured by the moving observer in the flow T.)

The flow determination technique discussed here was developed to be performed with waves propagating about 3 times faster than the flow, rendering wavelength changes on the order of 20%. The required equipment was designed to be relatively simple, inexpensive, and readily available.

The main parts of the research presented here are as follows:

1. Establishment from theory that surface flow in an area can be determined by the remote and synoptic mean of aerial imaging of at least two coherent wave trains (of known frequency and different directions) at the region of interest. All that is required for the flow determination is wave data at the region of interest. Information on the previous "history" of the propagation of the wave trains is not required. The results obtained here are based on linear wave theory and kinematic arguments.
2. Experimental observations and measurements of the effects of flows on coherent wave trains, for application in surface flow determination. These experiments were carried out both in an outdoors wave tank and in a local lagoon.
3. Analysis of the data obtained according to the guidelines of the theoretical investigation.
4. Investigation into practical aspects involved in the wave measurements, namely:

   the nature of specular reflection of sunlight from surface waves, as related to the accuracy of wavelength measurements from aerial photos of this reflection.

   This investigation includes an analytical model as well as experimental results, and was presented in the Oceans' 79 Conference. A copy of the paper read in that conference is in the Appendix.

In order to conduct the experiments, an outdoor experimental facility was designed and constructed. Experiments in waves, flows

and their interaction were carried out there under natural illumination. Transportable equipment to generate coherent wave train in harbors and bays was designed and constructed as well. The design of the wave generators incorporates some novel ideas to reduce wave noise.

Both the theoretical and experimental results of this work show that remote and synoptic determination of surface flow in harbors and bays by aerial imaging of coherent waves in the region of interest, works very well in the way outlined here. In addition, the aerial images of the waves are a compact storage medium for the synoptic surface flow data. The application of this flow measuring technique to the open ocean is discussed in the conclusion section of this thesis.

Waves in a flow

I will first review wave flow interaction where the linear waves and the flow are codirectional, along the lines suggested by Unna (1942). The constancy of period T_o for a monochromatic wave train in and out of a flow, with respect to a stationary observer, is expressed by the equation:

$$T_o = \frac{L}{C + U} = \frac{L_o}{C_o} \tag{1}$$

U is the speed of the flow, L, C, correspond to wavelength and wave phase speed in the flow, as seen by an observer moving with the flow. The o subscript denotes values in stationary water with respect to a stationary observer. Inserting the deep water linear waves dispersion relation

$$C = \sqrt{\frac{gL}{2\pi}} \tag{2}$$

(g is the acceleration due to gravity) into (1) and solving for C we get

$$C = \frac{1}{2} C_o \left[1 + \sqrt{1 + \frac{4U}{C_o}} \right] \tag{3}$$

Equation (3) can be expressed in terms of wavelength with the aid of equation (2):

$$L = \frac{L_o}{2} \left[1 + \frac{2U}{C_o} + \sqrt{1 + 4\,\frac{U}{C_o}} \right] \tag{4}$$

This is the wavelength seen by a stationary observer when the waves are in the flow. It is valid for slowly varying U(x). The more general occurrence when the waves propagate over a flow in any direction is treated below.

The relation: $L = C\,T_o + U\,T_o \sin\alpha$

has been known for some time (see, for example, Longuet-Higgens and Stewart (1961), equation 8.3, for an equivalent expression), and can be derived in many ways. Figure 2 aids in conceptualizing this relation by a simple Galilean transformation. L, $\bar{C}$, T, correspond to wave length, phase velocity and period of waves in the flow as seen by an observer moving with the flow. $\bar{U}$ is the surface flow velocity, α is the angle between the wave crest in the flow and the velocity $\bar{U}$. The o subscript denotes values in stationary water with respect to a stationary observer. U and C represent the magnitude of vectors $\bar{U}$ and $\bar{C}$.

First, we observe a small region in the wave crest from the viewpoint of an observer moving with the flow, and then modify this observation to obtain what is observed by a stationary observer. The moving observer measures waves passing with a velocity $\bar{C}$ in a direction perpendicular to the crest. As far as the stationary observer is concerned, observing the same waves inside the flow, the wave crest region has an additional velocity $\bar{U}$, and moves with a velocity $\bar{U} + \bar{C}$. After a period of Time T_o (T_o is the period of these waves measured by the stationary observer, independently of whether they propagate in stationary or moving water) the region of crest will propagate the distance $\overline{UT}_o + \overline{CT}_o$, shown as AB in Fig. 2. However, AB is not perpendicular to the wave crest. L, the wave length of these waves (observed by the moving as well as any other non-relativistic observer) is the perpendicular distance between the wave crests, denoted by A'B in Fig. 2, and $A'B = C\,T_o + U\,T_o \sin\alpha$, which is equation (5). (Wave energy propagates along $\overline{AB'} = \bar{C}T_o/2 + \bar{U}T_o$). Equation (5) can be

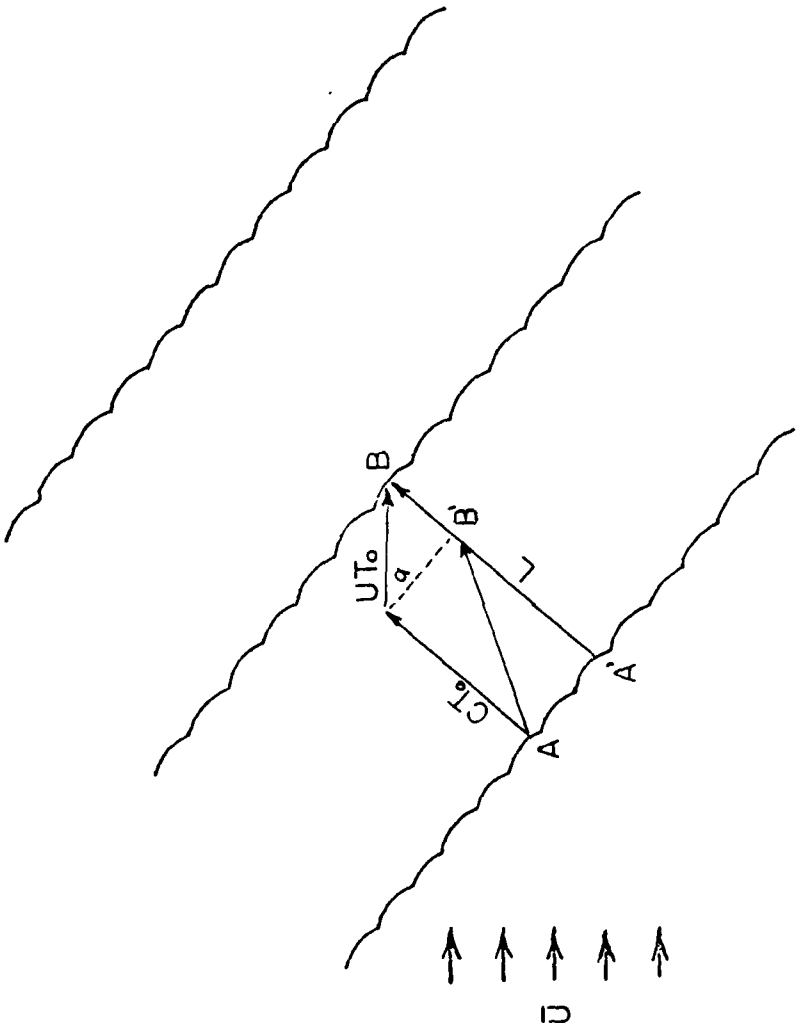

WAVES IN A CURRENT

Figure 2.

rewritten as: $U \sin \alpha = \frac{L}{T_o} - C$

with (1)

$$= L \frac{C_o}{L_o} - C \cdot \frac{C_o}{C_o}$$

and with (2)

$$U \sin \alpha = C_o \left\{ \frac{L}{L_o} - \sqrt{\frac{L}{L_o}} \right\} \qquad (6)$$

$U \sin \alpha$ is the component of the flow in the direction of wave propagation. Two such components of the flow, in different known directions, are required to uniquely determine the flow in direction and magnitude. It is clear from equation (6) that for the determination of the flow, the wave length and direction of each of two coherent nonparallel wave trains in the flow have to be determined. *A priori* knowledge of T_o (or C_o or L_o) of both wave trains is also required. Determination of the surface flow component according to equation (6) then requires wave data only at the region where the flow has to be determined. The "history" of the propagation of the coherent wave train before arriving there is not needed. Thus the waves can propagate through a complex flow pattern, and perhaps even reflect, before they arrive at the region of interest; as long as they remain coherent and the flow pattern is steady, flow measurements can be obtained. These probing wave trains can originate from a single point, provided they have different frequencies and different directions at the region of interest.

Equation (5) can be solved for L to describe the effect of the flow on the wavelength of the waves:

$$L = \frac{L_o}{2}\left\{1 + \frac{2U \sin\alpha}{C_o} + \sqrt{1 + \frac{4\ U \sin\alpha}{C_o}}\right\} \qquad (7)$$

This is plotted in Fig. 3. U sin α, as before, is the component of flow velocity in the direction of wave propagation in the flow. The one dimensional case is described by equation (4):

$$L = \frac{L_o}{2}\left\{1 + \frac{2U}{C_o} + \sqrt{1 + \frac{4U}{C_o}}\right\} \qquad (4)$$

By comparing equations (7) and (4) it is clear that the oblique case is reduced to a one-dimensional case by using U sin α as the flow in the direction of the waves. But in order to do so, it is necessary to first find α, the direction of the waves inside the flow, which amounts to solving the oblique case.

Shoals will significantly affect waves when the shoal is less than a quarter wavelength deep. Determination of slow to medium speed flows requires very short waves. An example will illustrate this point: a surface flow of one knot (50 cm/sec.) can be easily determined by waves with a wavelength in stationary water of L_o = 2m., propagating against the flow with an angle $\alpha = 45^\circ$. I chose here $\frac{U \sin\alpha}{C_o} = -.2$ in order to obtain $\frac{L}{L_o} = .52$ (see Fig. 3); thus in the flow L = 1 m. Shallow areas with depth of 50 cm in stationary water, and 25 cm in the flow region, that will affect the waves, are likely to be evident in the aerial pictures.

Measurement of fast flows of significantly more than a knot, requires faster and thus longer waves that may be affected by shoals. The effect of bathymetry and surface flows on the waves is different

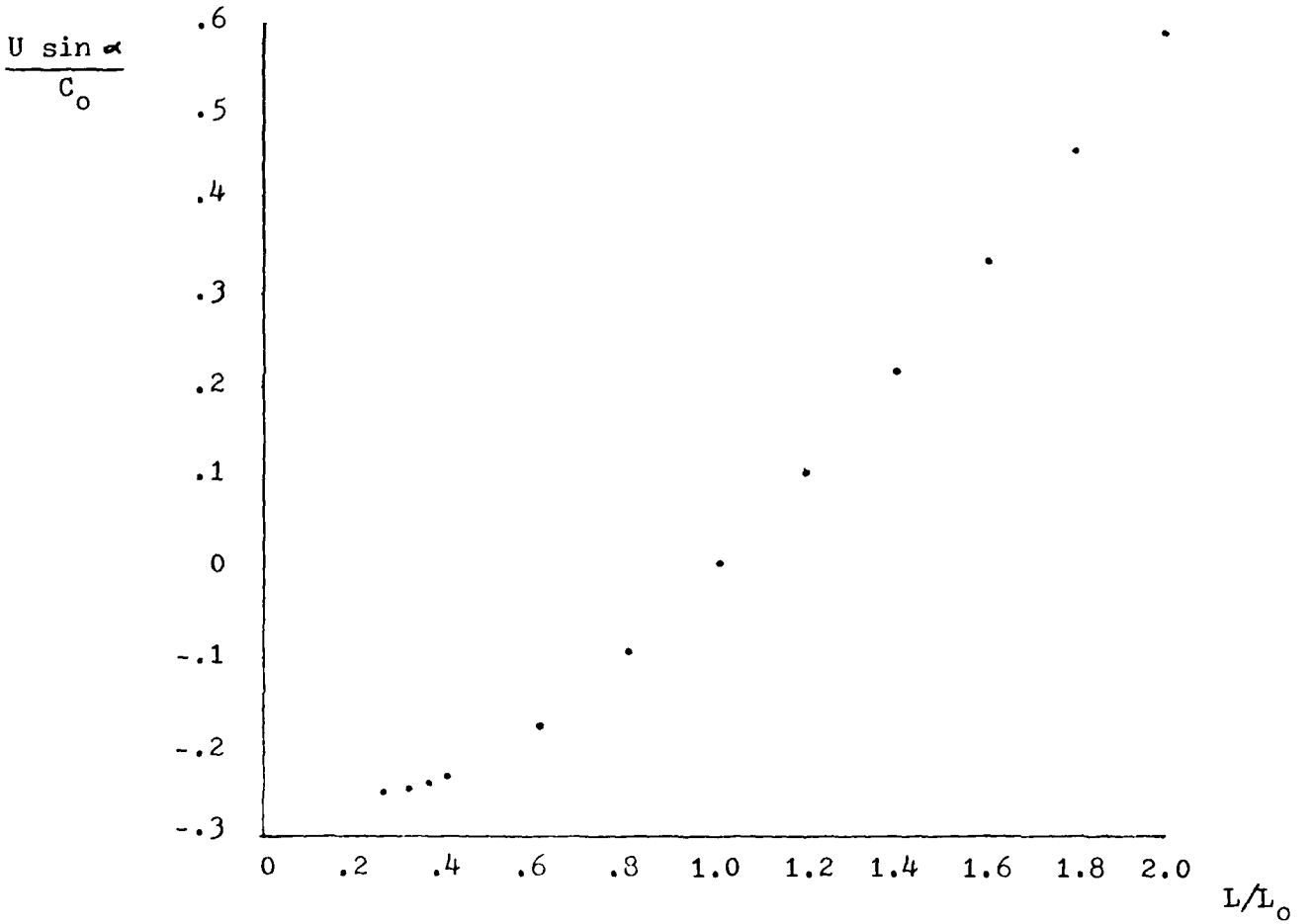

Figure 3

Velocity component in the wave direction as a function of wavelength

in the following way: bathymetry affects the waves, irrespective of their direction of propagation, analogously to the isotropic index of refraction of a medium in which light waves propagate. Surface flow effect on waves depends on the direction of the current flow with respect to the wave direction. When both current and bottom topography are thought to influence the waves simultaneously, their effects can be separated: probing with longer period waves shows larger wavelength changes, compared to their deep water value due to bathymetry, and smaller effects due to surface flow, and vice versa. Thus intelligent variation of the period of the generated waves can show whether bathymetry has an effect on the measurement, as well as supply qualitative inform-tion on regions of wave reflection and breaking that will help in establishing the surface flow distribution.

Generally, when short waves are available, such as with artificially generated waves in harbors and bays, synoptic flow measurements can be carried out in relatively shallow water. Figure 3 can help in establishing the range of wavelengths that can be used to probe the flow.

Distinguishing the effects of vertical shear from the effects of bathymetery is not as clear cut. Linear vertical shear will affect both long and short waves in a similar way, as long as the shear extends to depth of the order of half a wavelength. Thus vertical shear will affect long waves, when flows occur somewhere in the water column, less than half a wavelength deep. The effect of vertically nonhomogeneous flow on the phase velocity of codirectional waves was

explored by a number of workers, e.g. Biesel, (1951), Dalrymple (1973) and was described by Stewart and Joy (1974) as:

$$C = C_1 + 2k \int_{-\infty}^{0} U(z)\exp(2kz)dz \qquad (8)$$

C is the wave velocity on the flow, C_1 is wave velocity when there is no flow, k is wave number, U(z) is flow velocity, and the surface is at z=0. Deep water is at $z \to -\infty$. (A number of equations in that paper have typographical errors). They have also shown that for a flow monotonically decreasing with depth, and a weak shear, the wave velocity will be modified by the value of the flow at a depth of L/12.5.

$$C - C_1 \simeq U(\frac{L}{4\pi})$$

It is of interest to find out the effect of a layer type flow that has a maximum at depth D on the velocity of the surface waves. Assuming the vertical flow profile to be Gaussian-like in shape, for example:

$$U(z) = U_o \exp\left[-\frac{(-z-D)^2}{(2g)^2}\right] \qquad (9)$$

where D is the depth of maximum flow and g is a measure of layer thickness.

Inserting the flow value (9) into expression (8), and utilizing the similarity of (8) to Laplace transform, I obtain

$$C-C_1 = U_o \cdot 4kg \cdot F(2kg) \cdot e^{-kD} \qquad (10)$$

where $F(x) = e^{x^2}\int_x^{\infty} e^{-v^2}\,dv$ $\qquad$ $F(x) \to \frac{1}{2x}$ for large x.

Values for F(x) can be found in mathematical handbooks (see for example, Handbook of Mathematical Functions, by M. Abramowitz and L. Stegun, Dover 1965, Fig. 7.1).

D =	.025L	.05L	.0625L	.1L	.125L	.166L	.2L	.25L	.5L	L
exp(-2kD) =	.73	.53	.46	.28	.21	.12	.08	.04	.002	$3.5 \cdot 10^{-6}$

Table 1

exp(-2kD) as a function of D

According to this model (expression (10) and Table 1) it can be deduced that a layer flow with a maximum speed deeper than .25L will have little effect on the wave speed, no matter how thick the layer is, as for D >.25L we obtain $C-C_1 < .04U_o$.

Such a layer like flow with maximum speed $-U_o$ at 10 cm depth, and layer thickness measure of g = 1 m, will modify the speed of 1 m waves by $C-C_1 \approx .3U_o$.

The flow measurement discussed here assumes stationary, or slowly varying flows. An approximate value for flow variability that can be tolerated can be obtained as follows: The distance between the wave generators (or any place where wave frequency can be accurately obtained) and the position where the flow is measured, is n wavelength. Thus the propagation time of the waves from the generator to the measuring site is about $n \cdot T_o$. During that time, the flow variation ΔU should be limited to, say, $\Delta U \leq .02C_o$*, C_o being the phase velocity of

*This limit is approximately the same as the limit $\Delta\sigma \leq .02\ \sigma$. σ is the

the probing waves. Hence the upper limit on the allowed flow acceleration is

$$\frac{\Delta U}{n T_o} \leq .02 \frac{C_o}{T_o} \cdot \frac{1}{n} \approx \frac{3.2}{n} \text{ cm/sec}^2$$

$$\text{or } \frac{\Delta U}{\Delta T} \leq 3.2 \frac{\text{cm}}{\text{sec}^2} \text{ / per wave}$$

This value is independent of the period of the probing waves. As an example, for flow variation on the order of 10 cm/sec during a time period of about an hour,

$$\frac{\Delta U}{\Delta t} = \frac{10}{3600} = \frac{1}{360} \text{ cm/sec}^2$$

The value of n for this example is $n = 3.2/\frac{\Delta U}{\Delta t} = 1152$ waves.

Experimental Facility

The basic aim of the experimental work described in this thesis was to test the viability of this flow measuring system. The experimental approach was to generate two coherent wave trains over a flow, while simultaneously measuring the flow with conventional current meters. The value of the flow determined from the two wave trains, by the method developed in this thesis, would then be compared to the value registered by the current meters. I have conducted such flow measurements both in an outdoor wave tank and in a local lagoon. These experiments required the design and construction of facilities and equipment. The design, material purchases and construction took a great deal of my time and I consider it an integral part of this

---

angular frequency, and $\Delta\sigma$ its variation. From Whitham (1966) we have $\frac{D\sigma}{Dt} = \frac{\partial}{\partial t}(Uk + \sqrt{gk}) = \frac{\partial U}{\partial t} \cdot k$ or $\Delta\sigma \approx \Delta U \cdot k$. $\Delta\sigma \leq .02\ \sigma$ is thus $\Delta U \cdot k \leq .02\ \sigma$, or $\Delta U \leq .02 \frac{\sigma}{k} \approx .02\ C_o$.

research. Following is a short description of the facilities and equipment, with emphasis on those that had some novel design features.

The outdoor wave facility includes an outdoor basin, wave generator, beach, facility for flow generation, tower for overhead photography, and various devices to monitor the experiments. The outdoor basin is 30'x8'x2' (a photograph of the basin is in Fig. 4). The wave generator can be used with a 4' or 8' paddle and can be moved in the basin to supply waves in any desired direction. Its other features are described below. The flow is generated by a 350 GPM pump with water coming into the pool through a special diffuser box 7' long, where the water turbulence is dissipated to a large extent. An intake diffuser box is located on the other side of the pool. The tower is mounted atop an A-frame that can be placed anywhere along the length of the pool. Thus vertical pictures can be taken of the waves and other "action" inside the pool. A simple way to measure wave amplitude and length was used in the experiments conducted in the pool. A long thin vertical grid was half-submerged in the pool along the direction of wave propagation. Pictures of the grid as the waves passed it supplied both wavelength and amplitude data. Figure 7 in the Appendix is a picture of the waves as they pass the grid. If the water were rendered opaque by nigracine black, for example, the outline of the waves on the grid would be clearer.

The first wave generator I used was an inner tube pushed in-and-out of the water by a human volunteer who was listening to a metronome for frequency control. This method worked well, especially with low wind conditions (see Frontispiece for typical results). The next wave

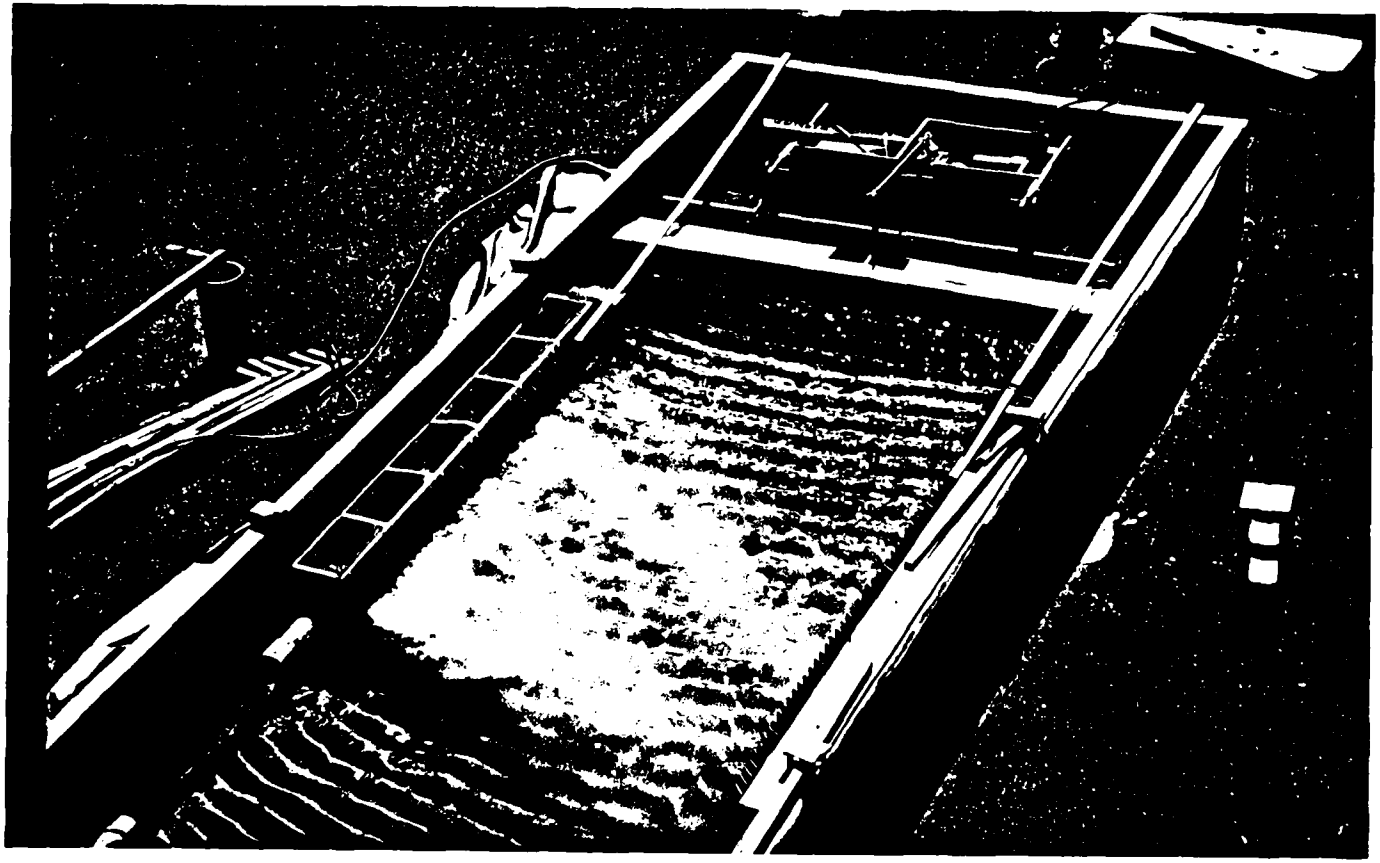

Figure 4.
Outdoor wave basin in operation.

generator design was for use in a wavetank and was portable as well. It was driven by a synchronous motor which was, in turn, controlled by a special electrical drive that maintained a fixed frequency. This frequency could be easily adjusted. In order to reduce noise by reflected waves in the wavetank, the paddle of this generator touched water on one side only and thus created waves moving to the front, none to the back. Figure 5a is a drawing of this generator and Figure 5b shows its capability. For wave generation in the lagoon, I used the same motor control discussed above to drive two paddles at the same frequency simultaneously. The paddles were placed in the water and the motor drive mechanism was on shore. A connecting rod and support rods attached the paddle to the drive unit. The paddle had a unique cross section; it is the same cross section that was suggested by Salter and Scan for the reverse function, to extract energy from waves in the ocean. The advantage of this paddle is that no waves are produced towards the rear, thus reducing the amount of wave noise. The whole wave generating system, including electrical generator, is transportable on a truck and thus could be used for various experiments in harbors, lakes or bays. This enables the utilization of natural illumination and there are no noise problems from waves reflected by the walls of wavetanks. Figure 6 is a picture of this wave generator.

An optical data processing system to help analyze the aerial photos of the waves produced in the lagoon was set up. It included a laser and lens arrangement that supplied two-dimensional Fourier transform of sections selected in the aerial photos. The system also included scale and direction calibration to enable fast and accurate

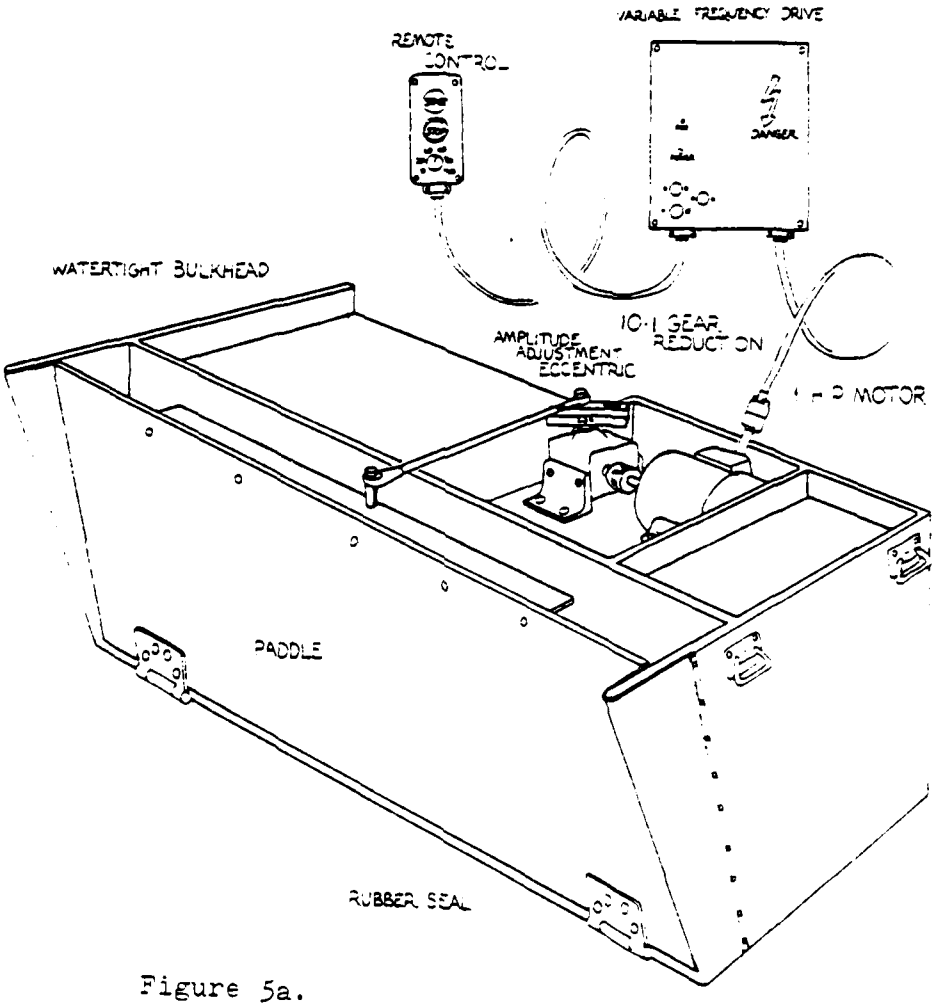

Figure 5a.

Wave generator

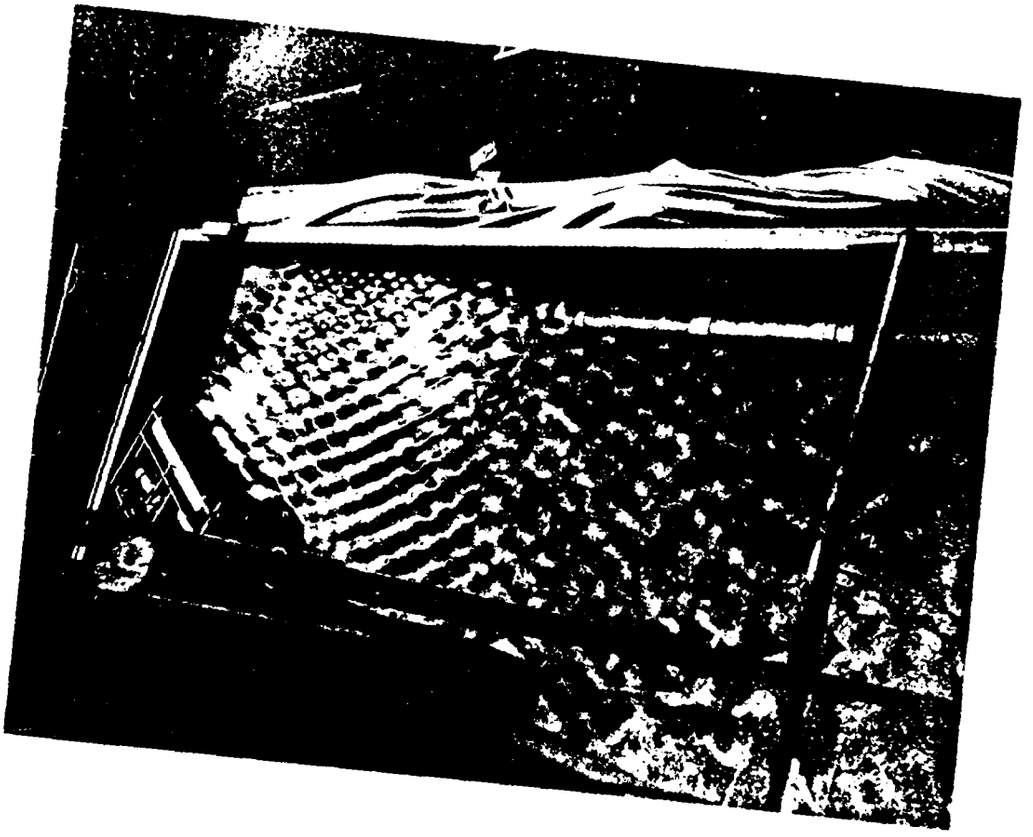

Figure 5b.

Wave generator in operation

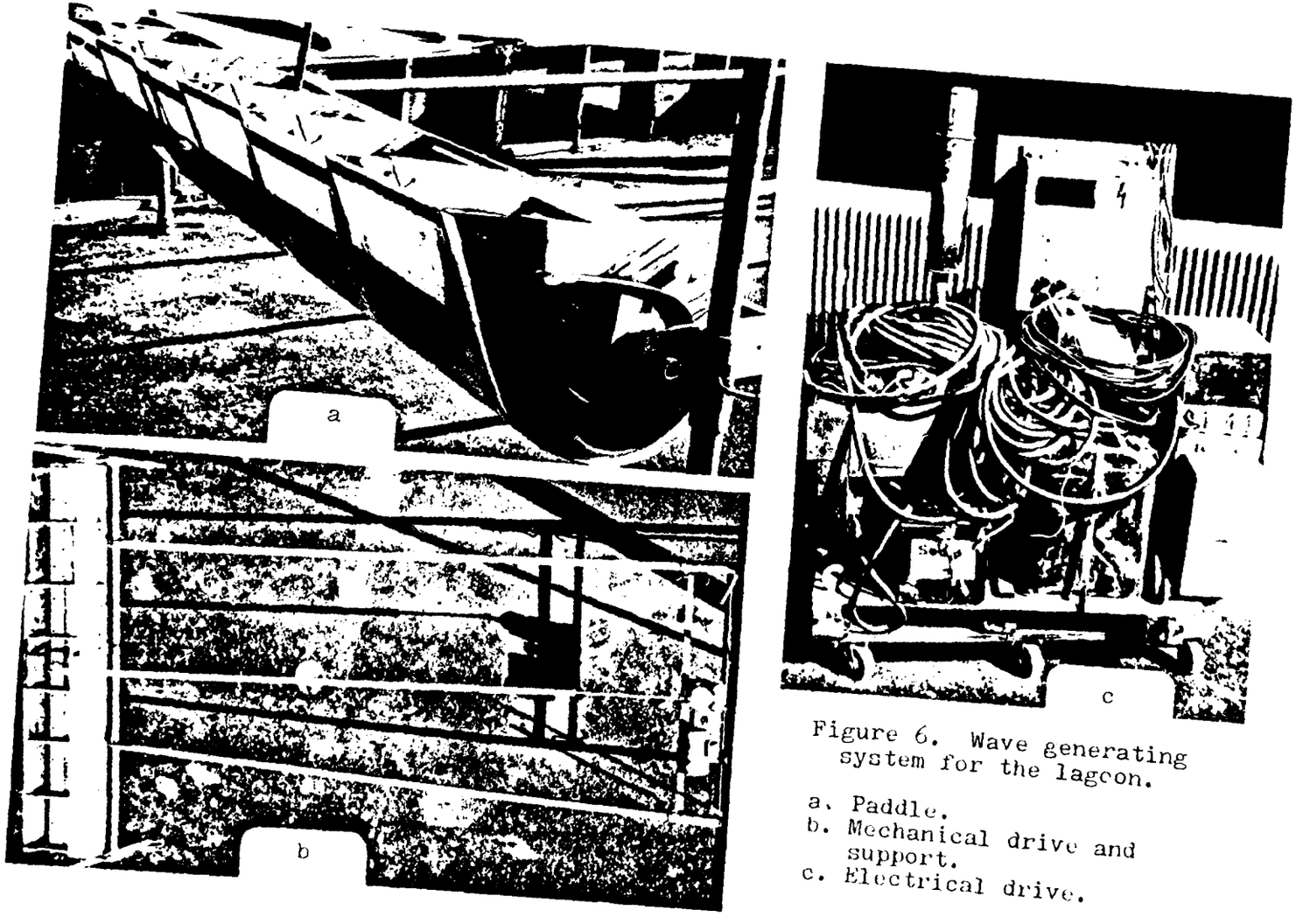

Figure 6. Wave generating system for the lagoon.

a. Paddle.
b. Mechanical drive and support.
c. Electrical drive.

flow determination from the aerial photos. A more detailed description of this system, which works well, is presented in the section dealing with data analysis.

Experiments in a Wavetank

The goal of the experimental work described here, was to correlate values of surface flow produced in the wave tank that were obtained from wave data in vertical photos of the wave tank, to surface flow values measured directly by floats. The production of homogeneous flow in a section of wavetank, for experiments in oblique incidence of waves into a flow, is not straightforward. The flow that I measured during this experiment varied from 6-9 cm/sec both spatially and temporally. Thus I view the experiments in the wavetank as something analogous to a shakedown cruise; this experiment qualitatively served to indicate whether something was amiss in the theoretical approach, and was also a guide in the operation of the complex array of equipment to be used later for an experiment in a natural body of water.

The experiment in the wavetank involved the following: Waves generated at a fixed frequency entered a surface flow at an angle. See Fig. 7 for a view from above the wave pool, waves, and two diffuser boxes for flow input and output. The specular reflection of the waves was photographed from an overhead tower, first with no flow condition (see Fig. 7), and then with full flow condition (see Fig. 8).

This experiment was carried out in October 1978 in La Jolla, and the sun is never in zenith there. Thus, in order to obtain

specular reflection from the waves the wavetank was photographed with the camera tilted in one axis at a carefully measured angle. During printing, the enlarger head, containing the negative, was tilted by the same angle as the camera. This resulted in prints that had the characteristics of photos taken vertically, that is, the film plane parallel to the water surface.

In this experiment, one generator only was producing waves that entered the flow obliquely. The component of the flow in the wave direction was calculated from the photograph, and compared to the flow component value obtained from independent measurement of the speed and direction of small submerged floats. Wavelength data from the photos was obtained (Fig. 7) by laboriously measuring the distance between specularly reflecting row couples in the pictures. The Appendix contains some background on the validity of such measurements.

The average of a number of measurements was used for the calculation of the flow. The results are presented in Table 1.

The results presented in Table I reflect the inhomogeneity of the surface flow in a relatively small wavetank. There was scatter in measured flow speed and direction by the floats. I regarded these results as qualitatively good and warranting larger scale experiments. Actually the value of the flow components measured by both techniques, as seen in Table I, was fairly close.

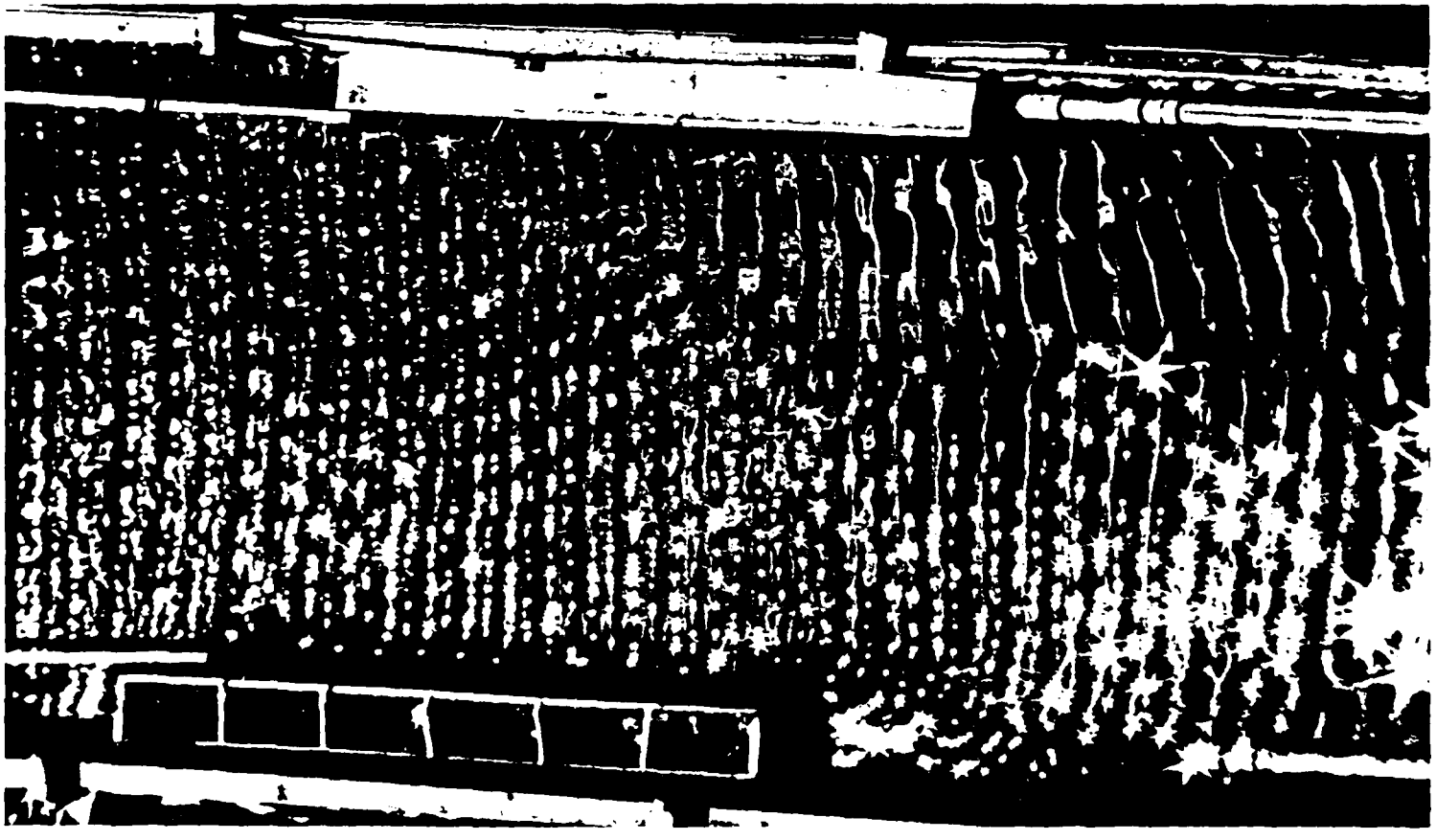

Figure 7.

Jacket in a wave tank, no flow.

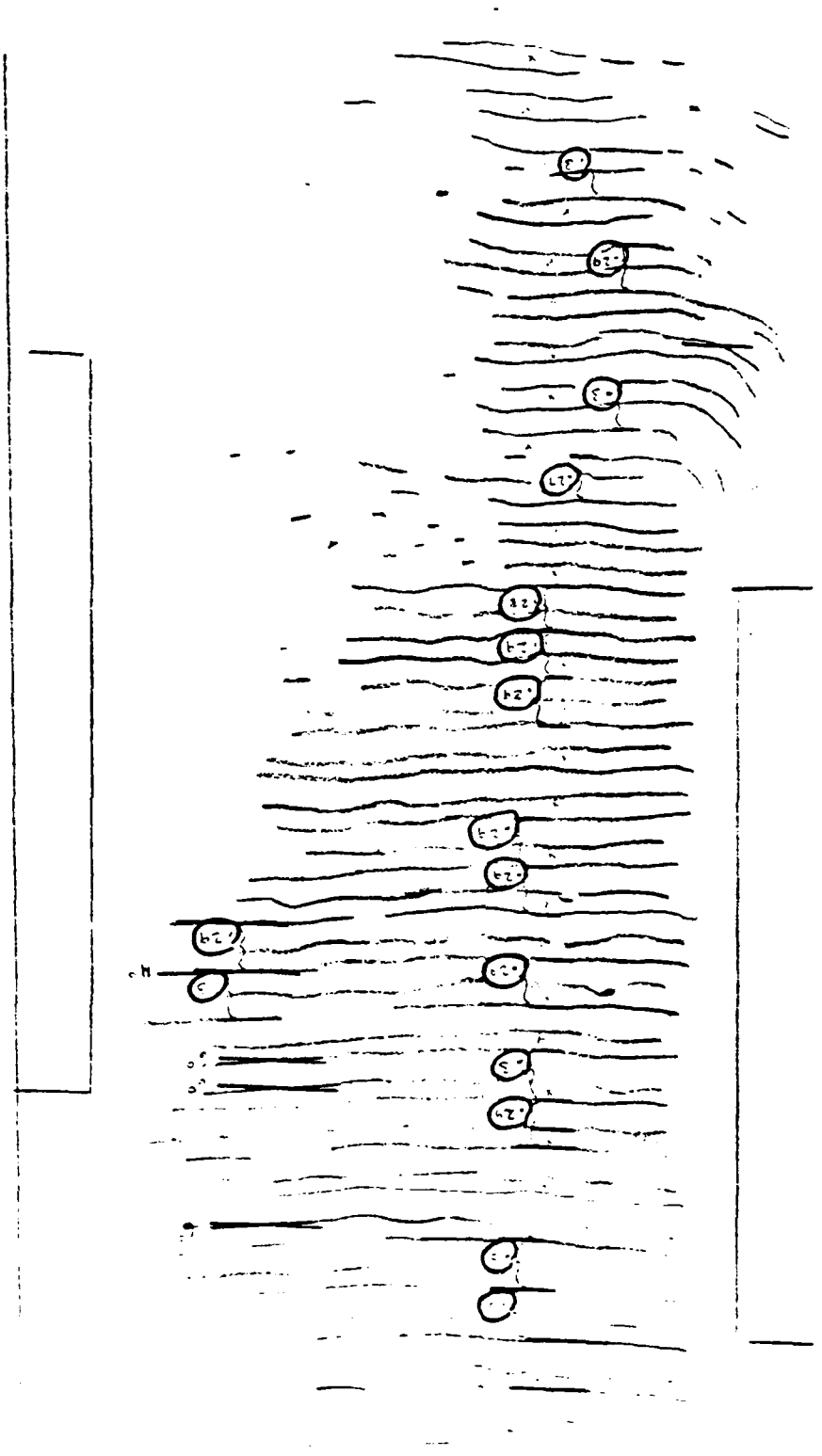

Figure 7a. Drawing of the wave crests.

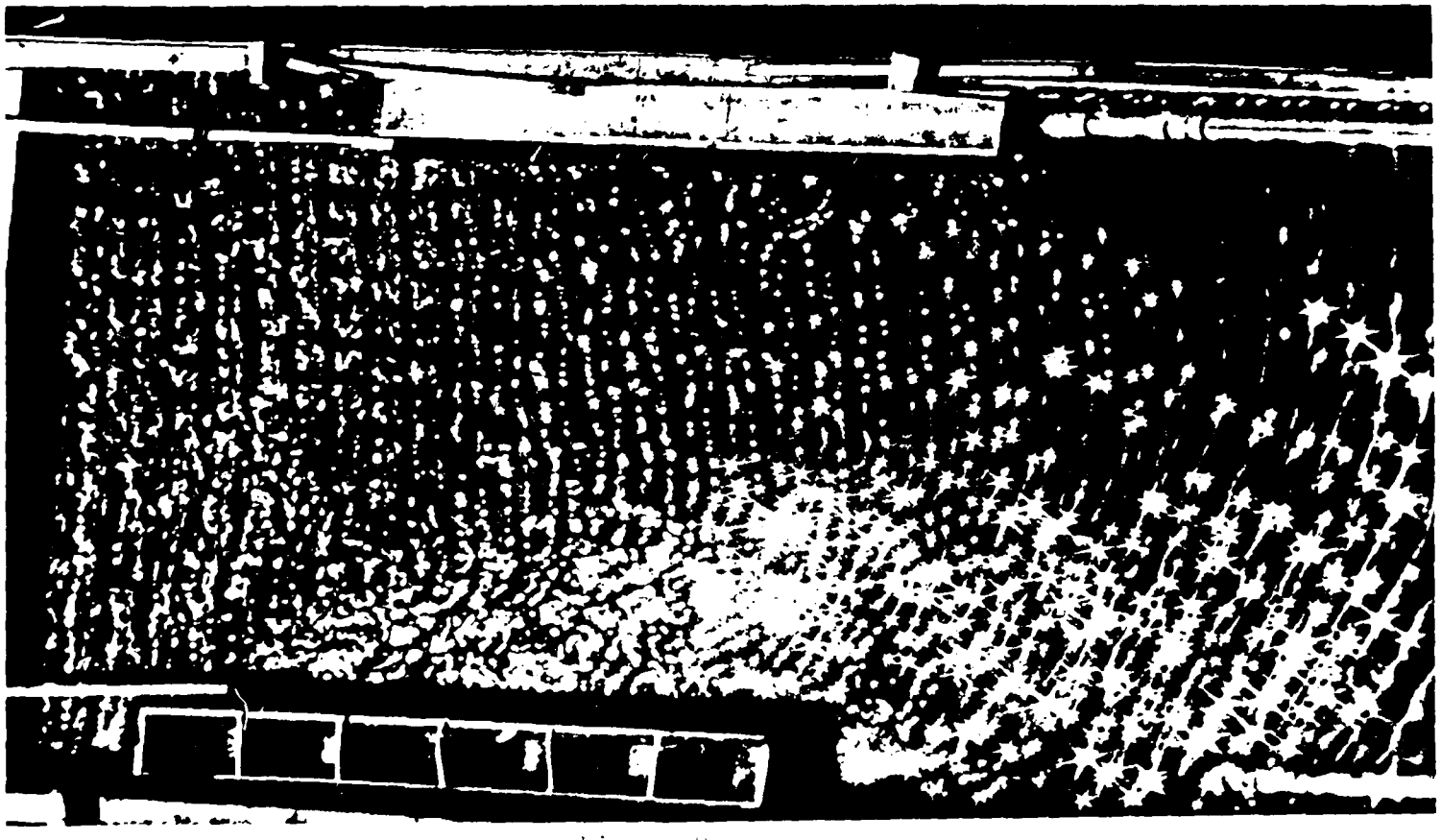

Figure 8.

... in the wave tank with flow from diffuser box at the bottom to box at the top of the picture.

Values measured in pictures of waves				Parameters measured with floats in the pool		
To Wave Period	L_o Average wavelength measured in pool region without flow	L Average wavelength measured in flow	u sin α calculated	U flow velocity	α angle between wave crest and flow direction	u sin α
.265 sec	.29"	.33"	3 cm/sec	6-9 cm/sec	$34^{\circ} \pm 10^{\circ}$	6 sin 24 = 2.4 7.5 sin 34 = 4.2 9 sin 44 - 6.25
.37 sec	.45"	.53"	5.4 cm/sec	6-9 cm/sec	$41^{\circ} \pm 10^{\circ}$	6 sin 31 = 3.1 7.5 sin 41 = 4.9 9 sin 51 = 7

Table 2

Comparison of Surface Flow Measurements in a Wavetank

(flow values in cm/sec.)

Investigation of surface flow in a lagoon by artificially generated waves

The purpose of measuring surface flows in a lagoon by coherent gravity wave trains propagating in them was to test the viability of this new measuring technique. The lagoon, Agua Hedionda in Carlsbad, Ca. (see Fig. 9), has a significant and periodically repeating surface flow pattern due to a power plant utilizing its water for cooling purposes and tidal flushing. The lagoon is 1000 m long and about 350 m wide with the long end oriented along 140°M. The power plant takes the water in from the southern tip of the lagoon and the connection to the ocean is in the northern end. On the east shore of the lagoon there is a connection to an eastern section of the lagoon.

The test was conducted by producing coherent wave trains from two wave paddles about 200' apart placed at the shore of the lagoon (they are described in a previous chapter) and photographing the lagoon surface from the air with a high quality camera looking vertically down. Savonious type current meters were placed in the lagoon at a depth of 60 cm to compare their data with the flow reading obtained from the aerial photos.

I have collected data during experiments carried out on January 19, 1979, and on June 19, 1979. More data was collected on the later experiment, so I will describe it first.

Preliminary considerations

In order to design the parameters of the experiment such as wavelength of the probing wave trains and position of the current

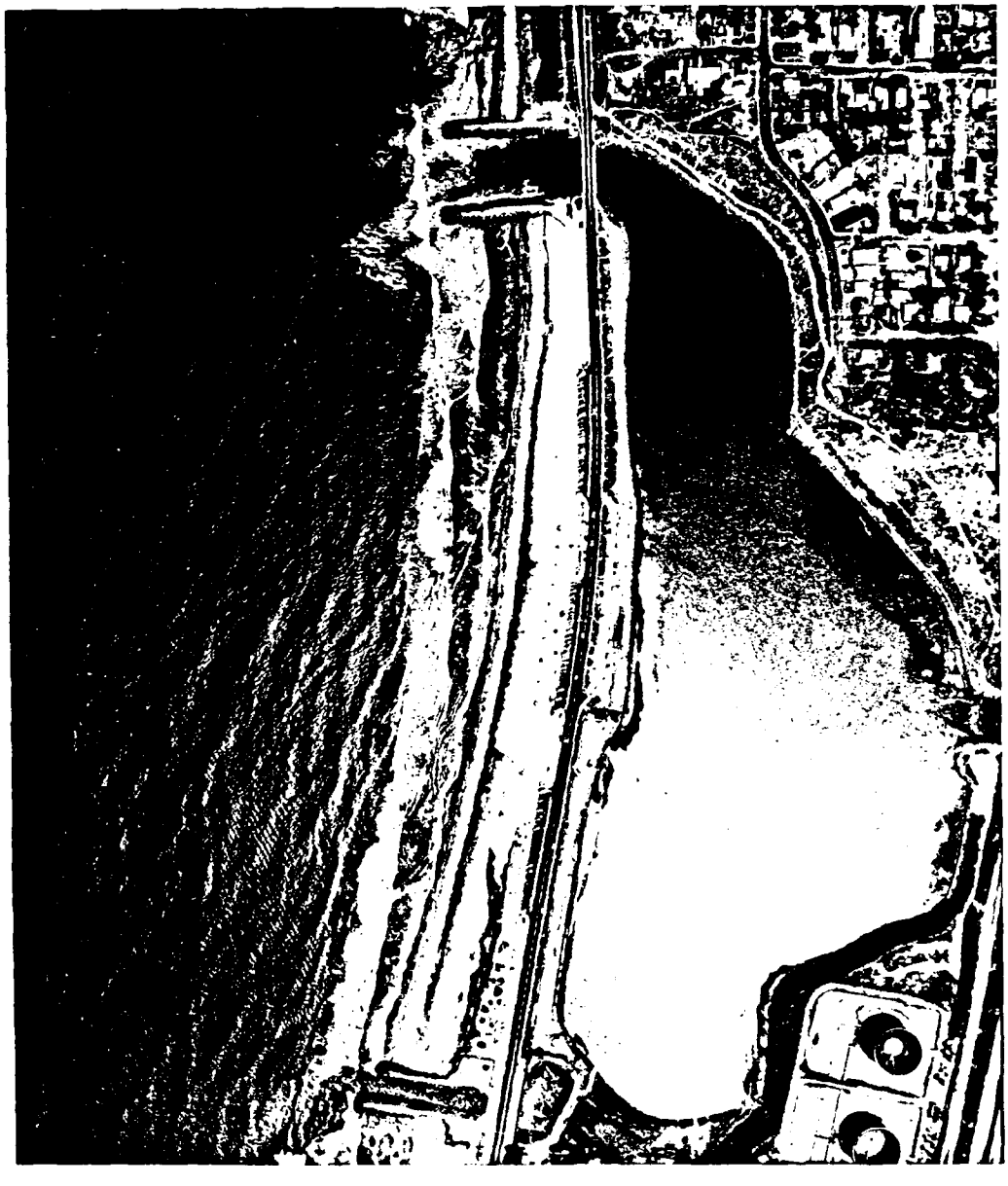

Figure 9.

The western part of the Agua Hedionda lagoon.

meters, I had to find out the approximate circulation of the lagoon, its variation with tidal cycles and powerplant operations, and an approximate bathymetry of the lagoon. I sampled the circulation of the lagoon by a handheld flow meter from an anchored boat, by savonious type current meters and by visual observation of different regions in the lagoon. The bathymetry was sampled with a lead line from the boat. The lagoon, which had been dredged a short time before the experiment, was deeper than 3.5 m in the area selected for the test (except nearshore). The surface flow in the lagoon varied between no flow to a few knots, depending on place and time. In the few measurements that I have, the flow at depth of 1' and 2' was mostly (but not always) faster than the flow at 6" depth. I chose a region that exhibited flow of about 20 cm/sec during ebb tide as the central region of our experiment. The required wavelength of the probing waves can be easily calculated with the aid of Fig. 3. This calculation shows that for a change in wavelength of about 20% due to surface flow, the probing waves need to be about 1 meter long.

In order to obtain high contrast wave pictures, the waves had to be "placed" in the edges of the region specularly reflecting sunlight into the aerial camera. The appendix describes the consideration of specular reflection of sunlight by coherent waves to an an aerial imaging device and the accuracy of the wavelength measurement from these pictures. These considerations suggest that the airplane should fly as high as permitted by the resolution of the camera (or other imaging device) and the wavelength of the probing waves. The camera should have a wide field

field of view, sufficient to image the waves near the specular region, with the sun at an angle away from zenith. I have obtained wave data from altitudes of 2000', 3000' and 4000' with a K17C aerial photo camera that has a 70° X 70° field of view.

Experimental work

The experiment involved generating waves in a lagoon by two wave generators, at the same time that surface flow was measured by current meters. The waves were photographed from the air. These photographs are the data (as well as the compact data storage medium) for surface flow determination. During the experiment there was equipment in the water (boat, current meters), on shore (wave generators and their drive systems), and in the air (airplane with aerial camera). All the equipment with people to control and operate it had to function well simultaneously. We have a few "dry runs" to test the experimental system. Not everything worked during those initial runs and I consider them educational experiences. One of the runs was conducted at night during full moon.

Following is a brief description of the main elements of the experiment.

I. Wave generators and their waves (see Fig. 10). The wave generators include two paddles placed in the water, with accurately controlled drive mechanism on shore. The waves produced by both generators in this experiment had a period of T_o = 0.76 sec (L_o = 0.9 m, C_o = 1.19 m/sec) as measured by a stopwatch and a tachometer. The generators were located about 200' apart on the western shore of the lagoon.

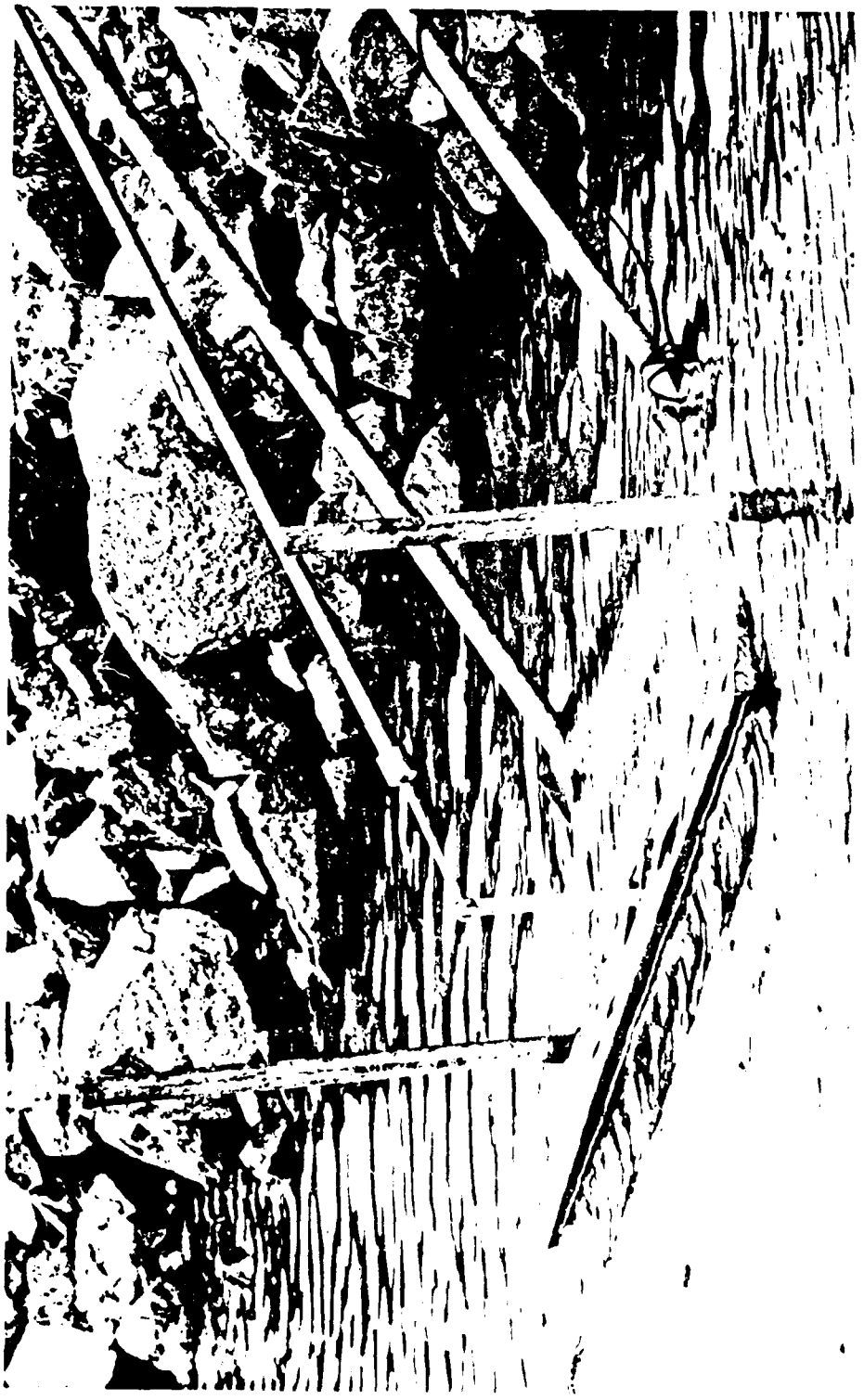

Figure 10. Wave generator operating in the lagoon.

II. Aerial Photography. Vertical pictures were taken with a K17C aerial camera at altitudes of 2000', 3000' and 4000'. The camera had a 6" focal length with a 9" X 9" film format (70 X 70° field of view). The best wave pictures were obtained at the edge of the specular region. Good pictures can probably be obtained closer to the "hot spot" with a reduced exposure. Resolution is good: a 2" diameter pipe can be seen in pictures taken at 3000'. Railroad rails can be seen across many of the photos taken. The image distance between the rails did not vary (to the accuracy of our measurement) between the center and the edges of the photographs, in a couple of photos that I checked, showing both good horizontal control of the photography and distortion-free imaging.

III. Current meters. We have data from 3 current meters placed from 110' to 220' away from shore. They are savonious rotor type, placed at a depth of about 60 cm. The flow indicated in them, at the time of the experiment, is 15-20 cm/sec. The flow direction indicated in two is approximately toward 140° magnetic; (in one current meter the compass did not cooperate).

The current meters show flow speed variation, in some cases up to 25%, in a time span of 3 minutes. The flow direction fluctuates according to these current meters, about ± 20° from the average direction within a period of a few minutes. In addition to the above current meters, I planned to use drifters, photographed from the aircraft at fixed intervals of time, for measuring the flow close to the surface. Unfortunately, the drifters (floating frisbees courtesy of Whamo Corp.) arrived after the experiment was completed.

Data

The data obtained during the experiment that was carried out June 19, 1979 includes aerial photos of the coherent wave trains and current meter data taken simultaneously. An example of the aerial photos is shown in Fig. 11. Slides were prepared from the negatives of the aerial photos to be optically processed, in order to obtain the wavelength and direction of the two coherent wave trains in any region of the lagoon, that was illuminated by the waves. Direction and length reference were incorporated in the slide. The following chapter has a detailed description of the optical data processing.

The current meter data was on chart paper of a russtrack recorder; it was timed and thus was correlated with the timed aerial photos. The position of the current meter was determined by additional vertical aerial photos taken from an altitude of 1000'.

The period of the waves was measured with a tachometer as well as a stopwatch. These measurements were repeated a few times during the experiment with no observable variation of the period. The water level of the lagoon exhibited variation with an amplitude of a few inches and a period of about one minute. These periodic surges, that may have been due to lagoon seiching triggered by ocean waves, caused amplitude variations of the waves produced by the wave generators. As a result, in the aerial photos of the lagoon the wave contrast is not constant.

Figure 11. Waves containing flow data.

Data processing

35 mm slides prepared from the 9" x 9" negatives of the aerial photos, were analyzed by a 2-dimensional Fourier transform. Goodman (1968) treats this subject in detail. I will briefly review here the way this transform is obtained. From early exposure to physics, we usually recall that when a beam of parallel and monochromatic light (usually, coherent laser light) passes through a regular diffraction grating, it splits into three beams of parallel light; one beam in the center is the same as the incident beam, only attenuated. The other two beams propagate at an angle α to the center beam, one beam above and one beam below the center beam; this assumes that the grating lines are horizontal. Figure 12 shows this particular case. The angle α is related to the spacing between the lines in the grating, d, by

$$\sin \alpha \simeq \alpha = \frac{\lambda}{d}$$

λ is the wavelength of the light beam. A lens placed in front of these beams will cause them to focus at a distance f, the lens focal length, away from the lens. These three bright focused points in the focal plane of the lens are the Fourier transform of the grating ℓ-the distance of each of the two points away from the center, to the center, is

$$\ell \simeq \alpha \cdot f = \frac{\lambda f}{d}$$

thus ℓ is inversely proportional to the spatial "wavelength" of the grating.

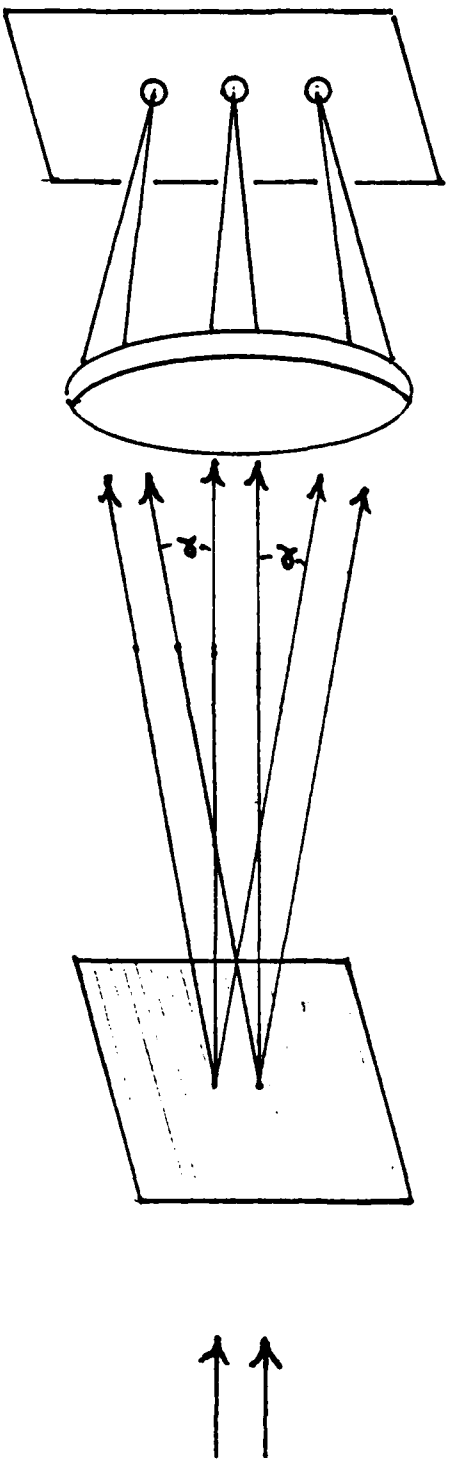

Figure 12. Diffraction of light by a grating.

The relevant mathematical relations of the Fourier transform are described in Fig. 13. The lefthand column presents the different functions, and the righthand column presents their Fourier transforms. The following property of the Fourier transform is used here: the Fourier transform of a product of two functions equals the convolution of the transforms of the individual functions. In simple mathematical notation this is written:

$$F[g_1 \cdot g_2] = F[g_1] * F[g_2]$$

F[g] is the Fourier transform of the function g.

In rows A and B of Fig. 13 are presented the one-dimensional sine wave and rect functions and their transforms. Row C has the product of a sine wave and a rect function, and their transform. In rows D and E are presented the two-dimensional equivalents of the above, produced by a lens. In D is presented the two-dimensional circular rect function (the aperture of the lens) and its transform, the focused point. In E is presented a sinusoidal grating and its transform, the two-dimensional equivalent of row C. The coordinates of the Fourier transform are in spatial frequencies - q, p. In the Fourier plane distances are measured in units of length x_f, y_f. The conversion factor is $x_f = \lambda \cdot f \cdot q$, $y_f = \lambda \cdot f \cdot p$, where λ is the wavelength of the laser light and f is the focal length of the transforming lens. A slide produced from a photo of the surface of a body of water covered with waves behaves in a manner similar to a number of superimposed gratings, oriented in different directions. The light energy diffracted by a coherent wave train will be focused in small

---

* means convolved with

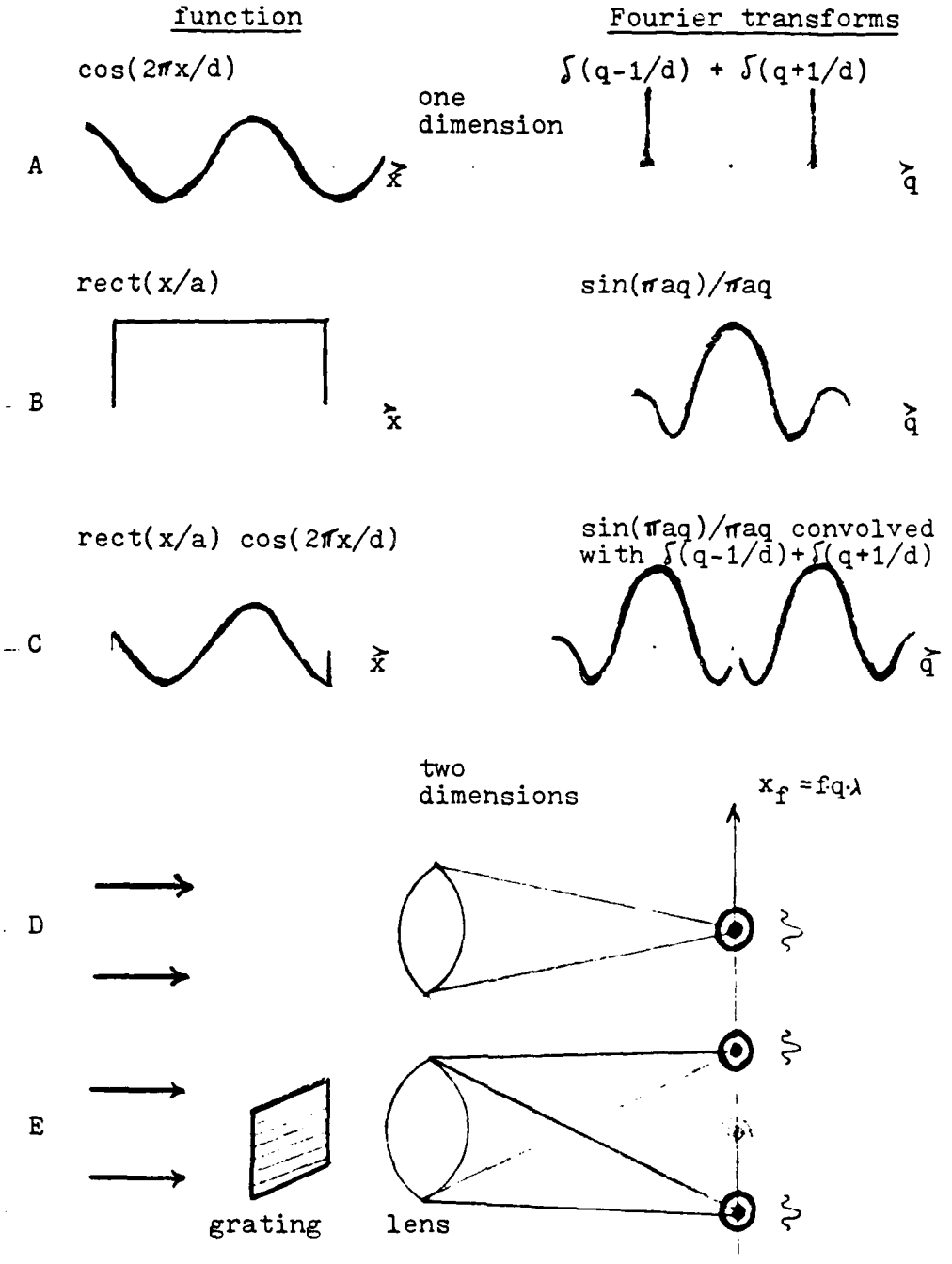

Figure 13. Fourier transforms

bright spots in the Fourier plane. Random waves will scatter the light energy of the beam over large regions of the Fourier plane. This will increase the signal (coherent wave train) to noise (other waves in the region) ratio for the actual measurement that is of interest to me, namely the spatial "wavelength" of the grating which is proportional to the wavelength of the coherent wavetrain.

The direction of wave propagation is the direction of the line in the Fourier plane, that connects the two bright spots around the center. Reference direction and distance are required in order to evaluate the surface flow from the bright dots appearing in the Fourier plane.

This technique of 2D Fourier transform of aerial photos of surface waves is obviously attractive for the determination of directional wave spectra. Barber (1954) started this approach even before lasers became available. Stilwell and Pilon (1974), Ichiye and Sugimori (1974), Sugimori (1975) are only some of the researchers who worked in this field. For my work here all that is required are the wavelength and direction of the waves, data that are easily and accurately obtained by this method. Acquiring power spectrum from these pictures is much more difficult, as perhaps evident by the number of people who are working on it.

The resolution of the two-dimensional Fourier transform can be determined with the help of Fig. 13. The wavelength of two wave trains, with wavelength d_1 and d_2 can be determined, if their transforms are separated by at least $\frac{1}{a}$. a is the diameter of the area containing waves that is being transformed (see Fig. 13b, c, for

these transforms in one dimension). This area is determined by the aperture of the Fourier transformer.

The separation between the transforms of the waves measures $\frac{1}{d_1} - \frac{1}{d_2}$. Thus, for resolution between these wave trains:

$$\frac{1}{d_1} - \frac{1}{d_2} \geq \frac{1}{a}$$

$$d_1 \cdot d_2 \simeq d^2 \tag{13}$$

or

$$\frac{d_2 - d_1}{d} \geq \frac{d}{a}$$

Hence, the number of waves in the "window" being transformed - $\frac{a}{d}$ is a measure of the resolution. For example, when the aperture being transformed contains 20 waves, $\frac{a}{d} = 20$ and $\frac{d_2-d_1}{d} = \frac{1}{20}$, or waves will be resolved that have a 5% difference in wavelength.

The directional resolution of the Fourier transform can be similarly determined; two wavetrains of the same wavelength-d, propagating in two directions $\Delta\phi$ radians apart can be resolved if $\Delta\phi > \frac{d}{a}$. In the example above $\frac{d}{a} = \frac{1}{20}$, and the directional resolution is $\frac{56^\circ}{20} \simeq 3^\circ$.

The shape of the bright spot in the Fourier transform contains information about the range of wavelength and direction in the observed wavetrain; a radially elongated spot indicates the range of wavelength for the wavetrain. An arcuate shape spot in the θ direction indicates the directional range of that wavetrain. The wavelength and direction determined from a "smeared" bright spot, is in some sense an average of these parameters of the wavetrain being processed at the

aperture of the Fourier transformer.

The optical setup required to obtain a Fourier transform is shown in Fig. 14. One of the Fourier transforms of the two coherent wave trains in the lagoon is presented in Fig. 15.

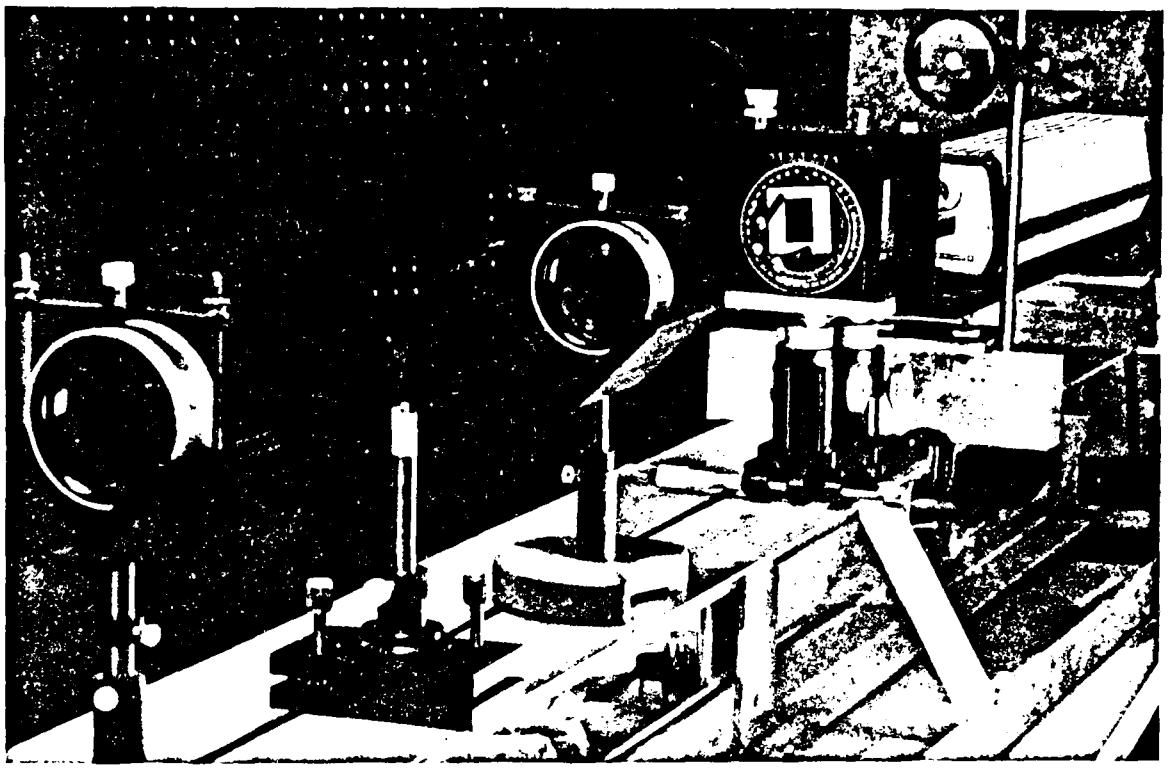

Figure 14. 2D Fourier transformer.

The laser is at the extreme right. Next to it is the data slide seen in a holder that enables calibrated movement in the X,Y,θ, directions. Next to the slide is the Fourier lens. The second lens on the left images the Fourier transform onto a Polaroid plate holder (not shown). Between the lenses is a small filter that attenuates the center beam of the Fourier transform.

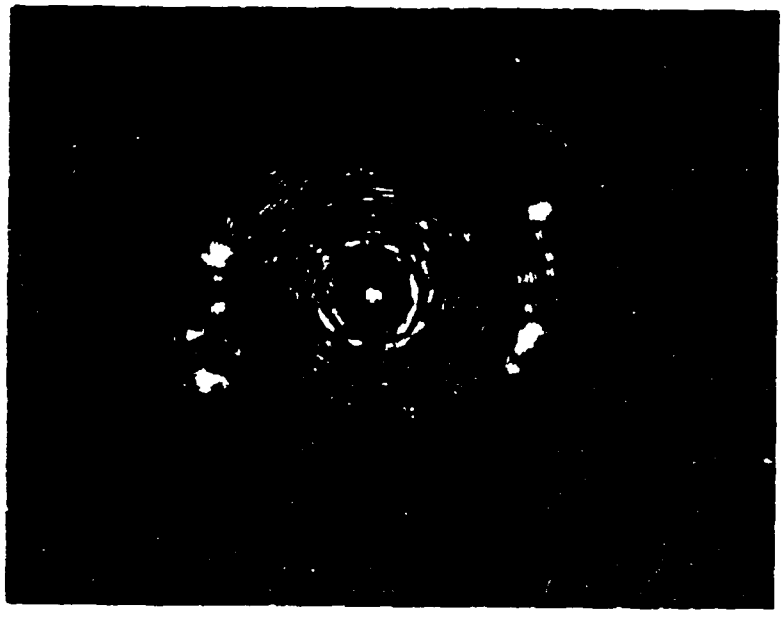

Figure 15.

Optical Fourier transform of a small region in an aerial photo of the waves in the lagoon.

Processing of the data obtained on June 19, 1979

The wave data is contained in a number of 9" x 9" photographs of the waves in the lagoon. 35 mm slides were taken of these pictures, together with angle and distance references. These slides were placed in the Fourier transforming setup (see Fig. 14) resulting in a 2 D Fourier transform, with an example shown in Fig. 15. Careful measurements of the distances and angles between the bright spots in the transform, as described in the section on data processing, enabled determination of the flow components. The resultant flow velocity was determined by these components with the help of a drawing. I would like to point out here that these computation steps can be achieved efficiently by the use of a computer and a display, employing available hardware and software.

The aperture used in the 2D Fourier data processing encompassed 10-15 waves, thus enabling resolution between waves that have wavelength differing by 7 to 10 percent (see section on Data Processing for an explanation). The determination of the wavelength of a single wave train is more accurate than the above 7-10%, as it involves finding the center of a bright spot, whose diameter corresponds to the 7-10 percent ambiguity in wavelength. I expect a 3-5% accuracy in wavelength measure to be a reasonable value. To assess the effect on flow measurement of ambiguity in wavelength, I take the derivative of equation 2:

$$\frac{\partial(U \sin \alpha)}{\partial L} = C_o\left(1 - \frac{1}{2}\sqrt{\frac{L_o}{L}}\right)\frac{1}{L_o}$$

For a rough approximation of this value I will use $\sqrt{\frac{L_o}{L}} \approx 1$ $C_o \approx 2.5U$

$$\text{Hence, } \frac{\Delta(U \sin \alpha)}{U} \approx 1.25 \frac{\Delta L}{L_o} \qquad (11)$$

or a scatter of 5% in wavelength data corresponds to an ambiguity of $1.25 \cdot 5\% = 6.25\%$ in the determination of the flow component in the wave direction.

In the 2D Fourier transform setup, the aperture was placed by the slide, in positions where the current meters were located. The position of the current meters was determined from low altitude vertical photos of the lagoon, when the area photographed was out of the specular region. Due to positioning inaccuracy, the area processed by the 2D Fourier transformer may be up to about 10 m away from the position of the current meters. There were five current meters in the lagoon waters; two current meters worked well, one showed only water speed (no direction), and two units did not operate, once introduced to the lagoon water. Thus each slide was processed to find the flow in three positions, where the current meters were in operation (see Fig. 16). Eleven pictures were processed, covering a time interval of half an hour. In a few positions, one or both wave trains were not visible. The data gathered from the position of current meter #5, both from the current meter and from the wave analysis, is presented in Fig. 17. The data is presented in the form of flow velocity (speed and direction) as a function of time. Similar results are presented for the position of current meter #1002 in Fig. 18, and the position of current meter #1 in Fig. 19. Current meter #1002 had shown no direction data. I assume though, that the flow direction there was on the average similar to that by current meter #5. In cases where a number of pictures were taken within less than a minute apart, or a

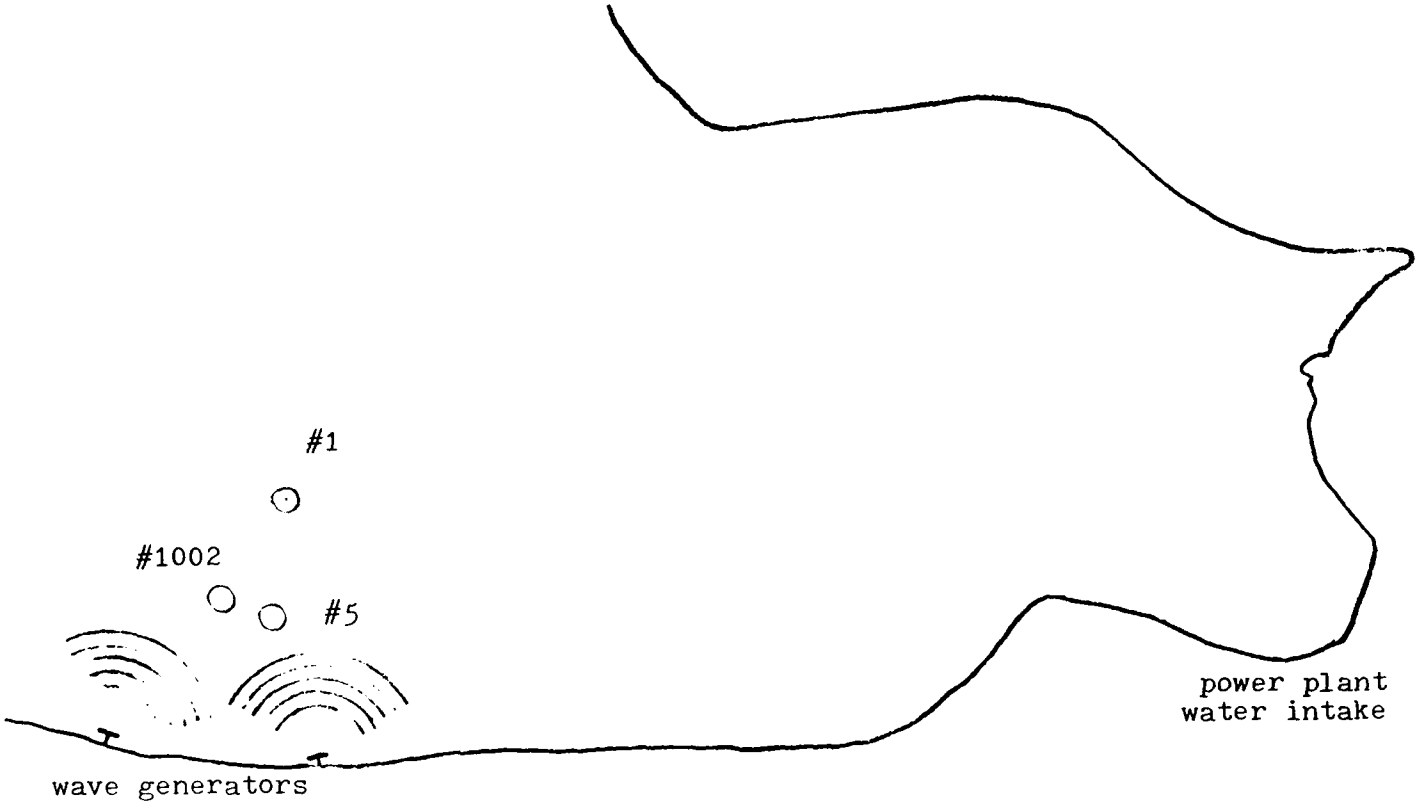

Figure 16. Location of current meters. Scale 1:2000.

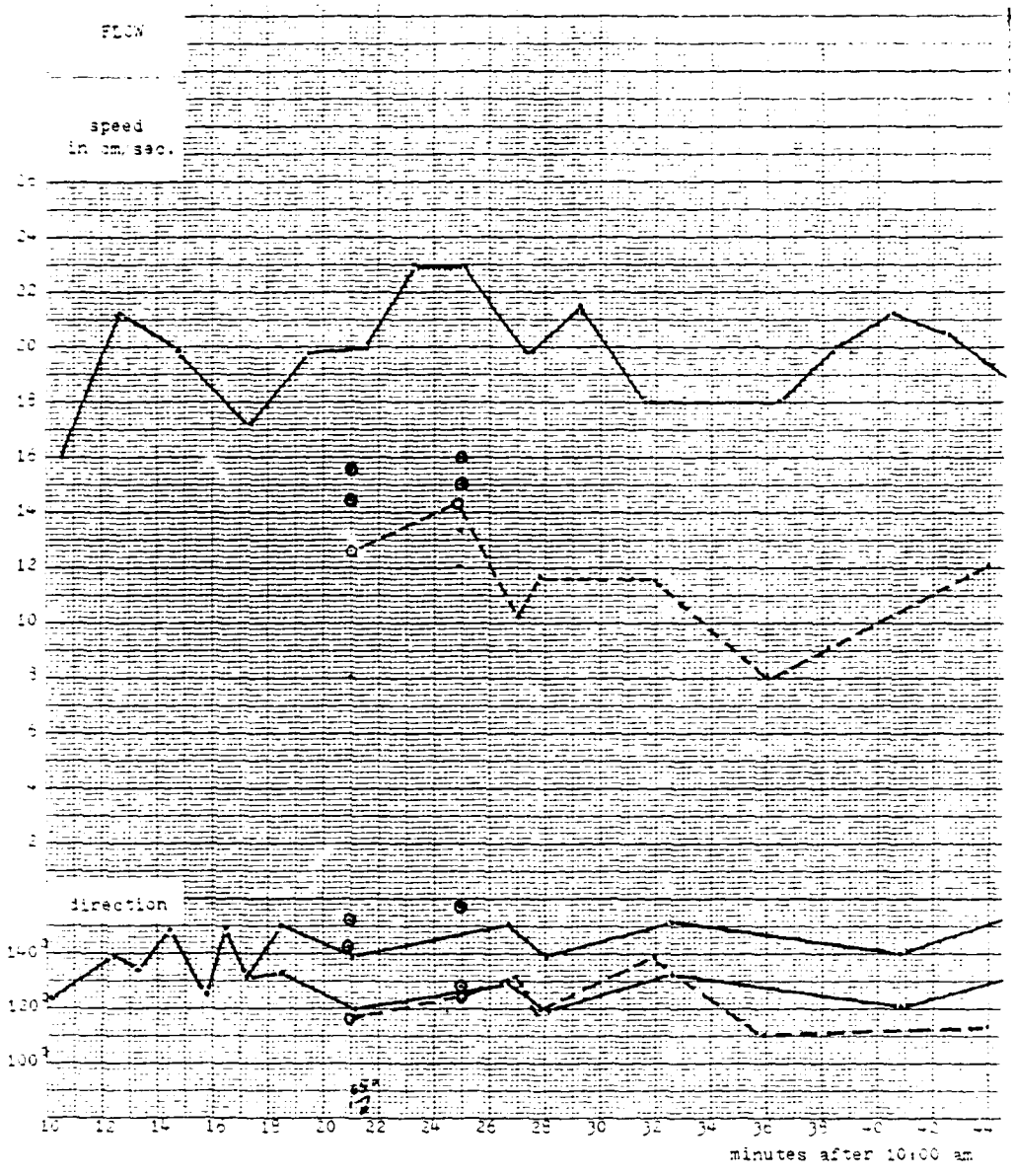

Figure 17

Comparison of flow measurements from current meter # 5 (solid line), and from wave data obtained by 2D Fourier transforms of aerial photos of the same region (broken line). Open circles are averages of the readings indicated by the black dots. Black circles around the dots indicate data processed with a magnifier.

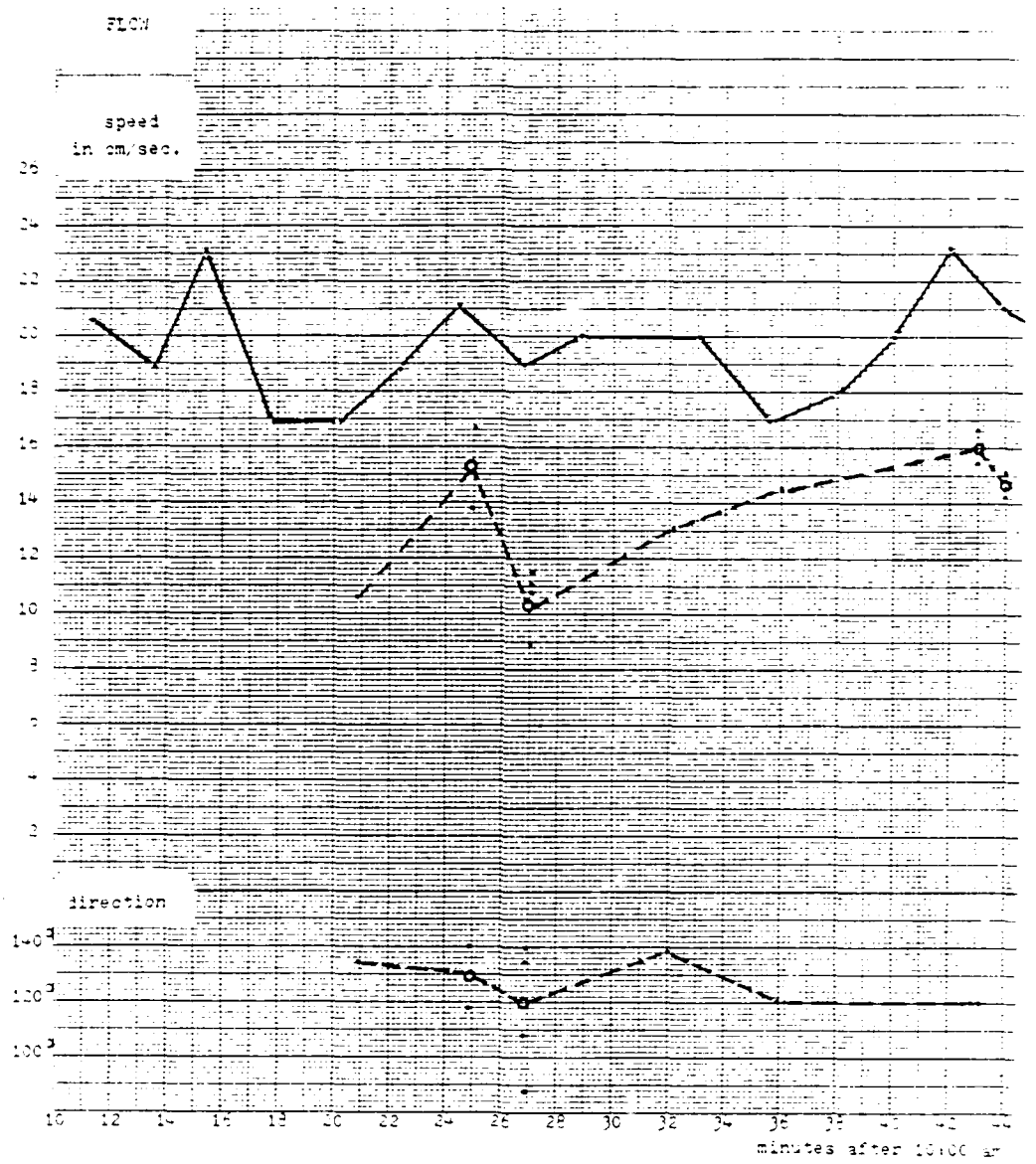

Figure 18.

Comparison of flow measurements from current meter #1002 (solid line), and from wave data obtained by 2D Fourier transform of aerial photos of the same region (broken line). Open circles are averages of the readings indicated by black dots.

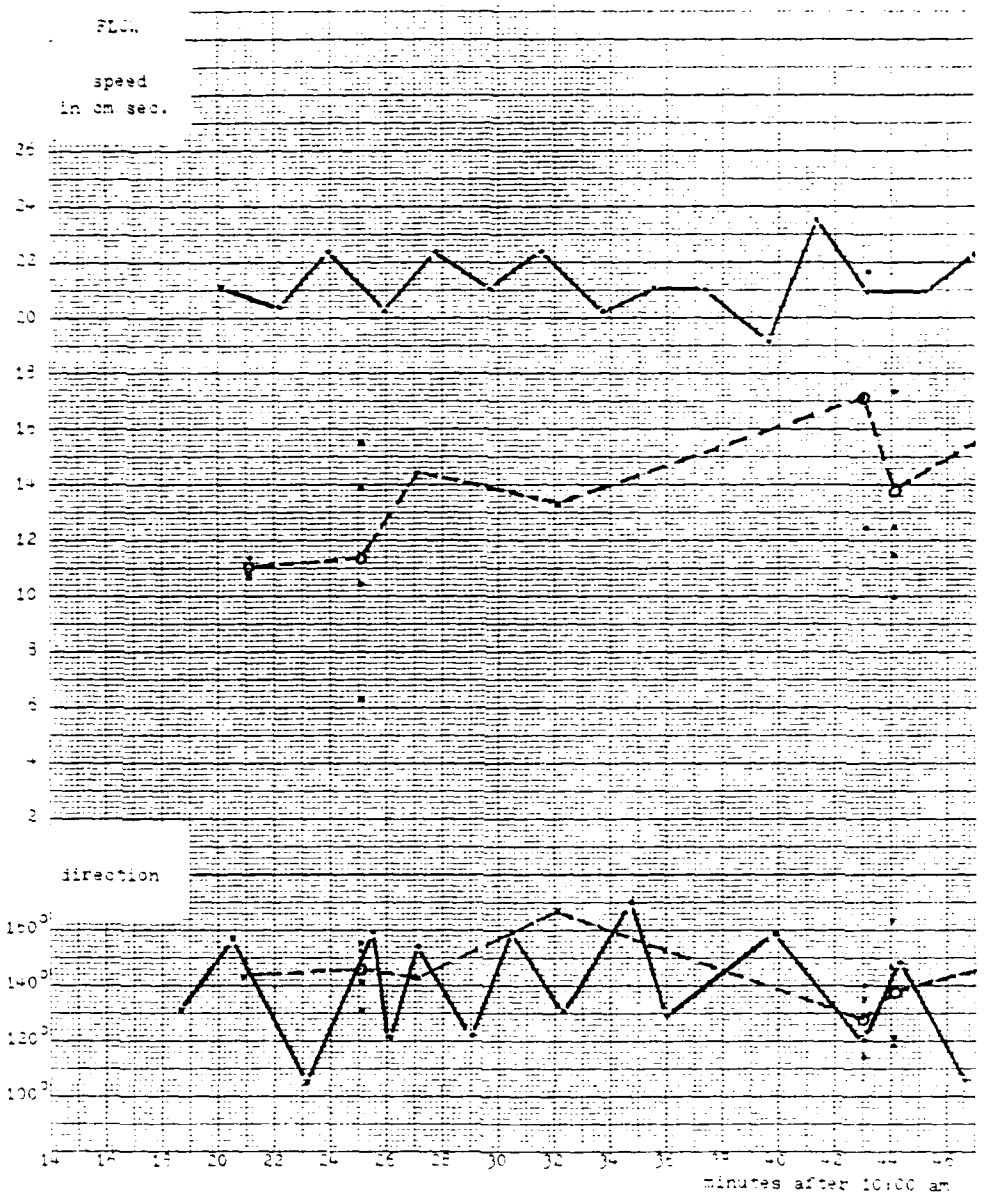

Figure 19.

Comparison of flow measurements from current meter #1 (solid line), and from wave data obtained by 2D Fourier transforms of aerial photos of the same region (broken line). Open circles are averages of the readings indicated by black dots.

few spatially close regions were processed for the same picture, the flow data is indicated and the average value presented as an open circle. In Fig. 17, I have included flow data points processed from aerial pictures by the laborious technique of using a magnifier with a scale, rather than the 2D Fourier transform. These points are indicated by a black circle; they are in good agreement with flow values obtained by 2D Fourier transforms.

A number of features are immediately obvious from the data presented in Figs. 17-19. The flow speed values measured by the wave data are consistently lower than the speed values registered by the current meters. The flow direction measured by both techniques are about the same. I will just note here that the current meters were placed at a depth of 65 cm (it is very difficult to deploy them any shallower than that), while the 1 meter waves that we used probed the water at depth of about 6" or less. (See chapter on accuracy in this thesis for elaboration). Another obvious feature is the wiggliness of the data, both in speed and direction. The sampling period, more than a minute in the current meters seems to be also the period of flow variation. A significant variation in flow values is observed in wave data that was taken by aerial pictures less than a minute apart, or analyzed from the same picture at slightly different positions, less than 15 m apart. There is evidence, discussed in the next section and in the Discussion section, that this variability is real, emphasizing the capabilities of this flow measuring system. Figure 20, which shows a number of flow readings processed from one picture along a line directed at 55°M also shows the spatial variability of the flow.

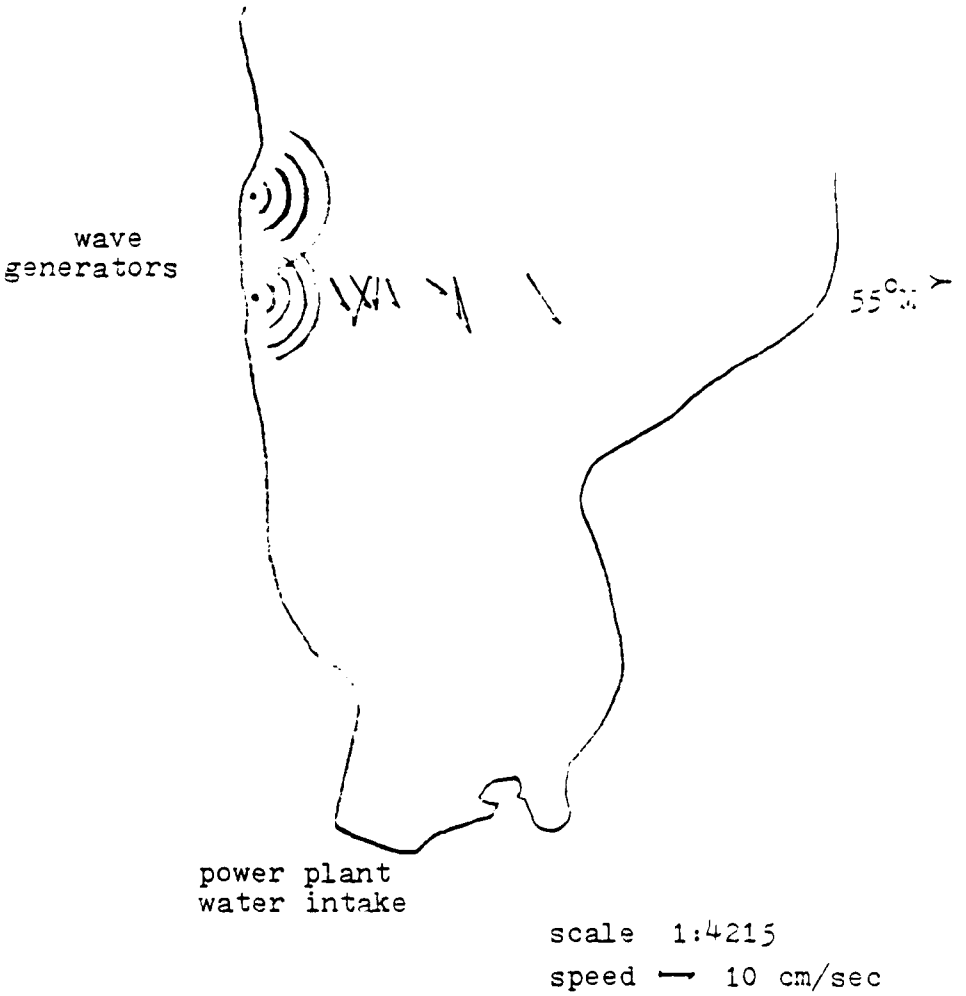

Figure 20.

Current readings along a transect directed towards 55°M, obtained from a single aerial photo.

More importantly, Figure 20 shows the synoptic capability of this flow measuring technique to obtain current readings from one aerial photo. A detailed analysis of the results is in the Discussion section.

Following is a description and analysis of data obtained on January 19, 1979.

Data obtained on January 19, 1979

On January 19, 1979, we had the same wave generating setup on the ground, as described in the previous chapter. One current meter was in the water, in the region where both wave trains were observed together. Photography was accomplished with a hand-held 35 mm camera tilted 45°. This tilt was rectified during printing by tilting the enlarger head by the same tilt as that of the camera. The pictures were taken from a small airplane at 1500' altitude. Figure 21 is the rectified picture used to obtain flow data. The picture was analyzed "by hand," by carefully marking the wavelength of the waves, averaging it for groups of about 5 waves. A micrometer stage with a pointer needle, together with a drawing machine, were used for this analysis, in order to obtain accurate variations of wavelengths with position. Figure 22 shows the variation of wavelength along three different propagating wave rays, as a function of position. The numbers marking position refer to numbers on the ray in Fig. 21. Each small square is one wave. The unexpected result here is the periodic variation in wavelength, with a period of about 30 waves. This may well be a reflection of flow variability, as water depth in the region was larger than half a wavelength.

The sampling rate of the current meters' flow data, that was used for comparison with the flow data from the wave pictures, was 12 per hour; thus the current meter was not suitable for measuring flow variability with temporal scales suggested by the wave data. The mean flow value obtained from the current meter could be compared to some average flow value obtained from the wave data. An approximation to

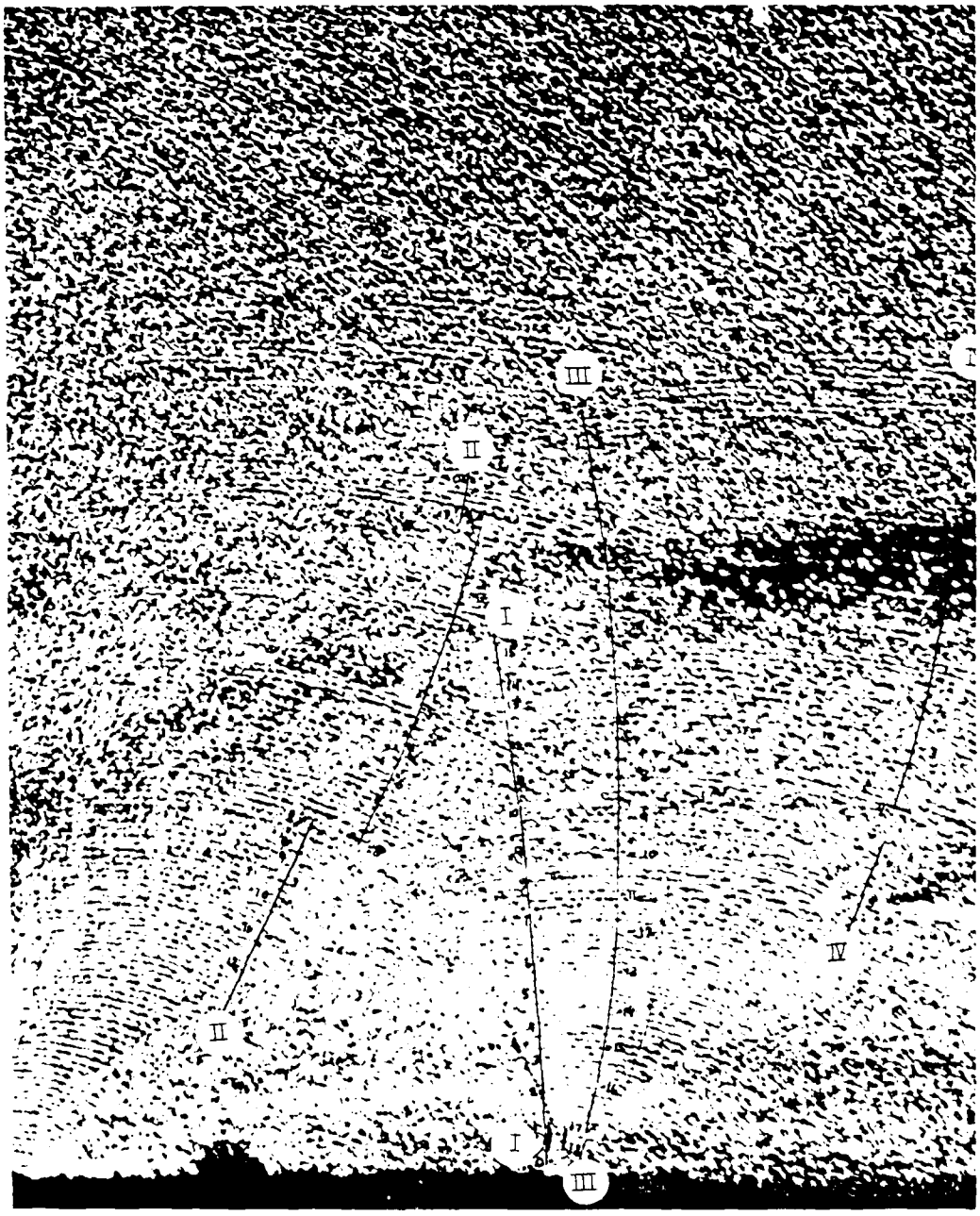

Figure 21. Wave data from January 19,1979.

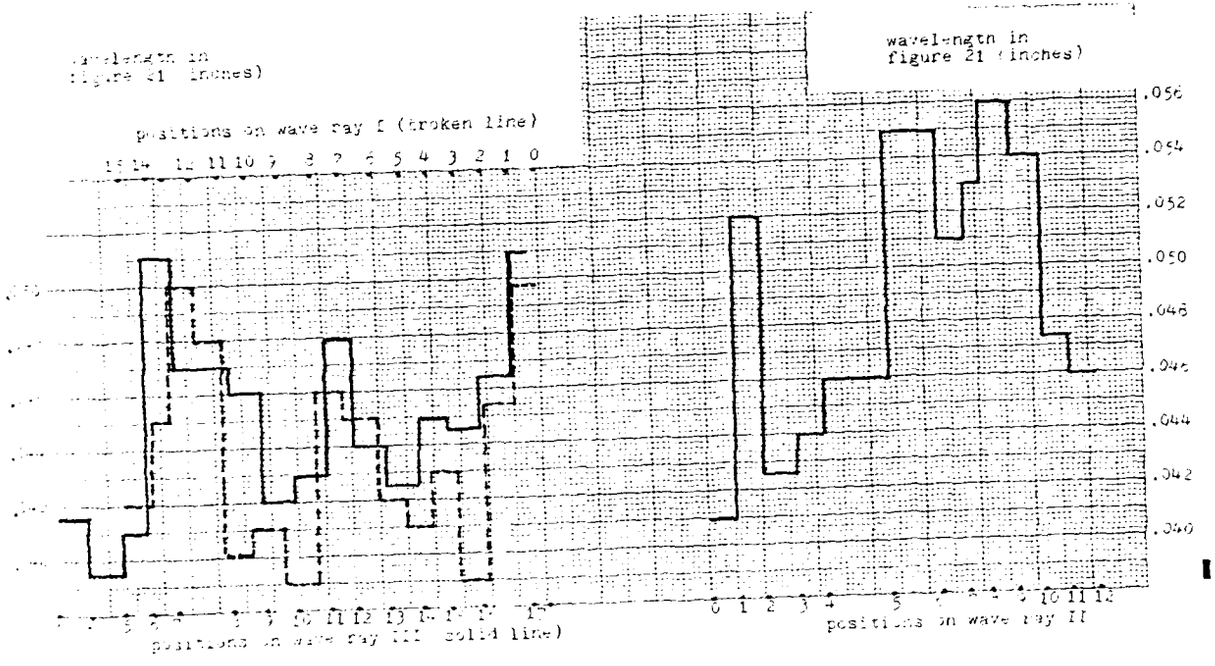

Figure 22.

Wavelength as a function of position for three different wave rays in figure 21. Each small square on the abscissa represents one wavelength.

the mean flow can be obtained by averaging the wavelength of the probing waves in the picture over the spatial scale of the variability. Utilizing this approach for flow measurement near the current meter (that was deployed about the middle of the wave covered region in Fig. 21) I calculated the average wavelength over 30 waves from Fig. 22, for wave rays I and II. The average value for ray I is .0435" and for ray II is .0466". The no flow wavelength calculated from Fig. 20, by subtracting 10% from the wavelength of the waves near the paddle (due to finite amplitude effect; 10% is the average wavelength increase near the paddle that I obtained for a few lagoon photographs with waves of known frequency) resulted in L_o=.0453".* The flow thus calculated, taking into account the direction of wave propagation, is 10.5 cm/sec towards 140°M. 140°M is along shore from north to south in this case, with the wave generators on the western shore of the lagoon in Fig. 20. Current meter reading for that time was 8 cm/sec directed towards 140° ± 10°M. Not only does the flow measurement by waves agree with the current meter reading, it also gives us some further insight into the dynamic processes of the lagoon. The periodic variation of wavelength shown in Fig. 22, and the successive bands observed in the waves about 15 waves apart in Fig. 20 as well as in Fig. 9, are manifestations of some processes that may be of interest in remote observation of bodies of water. The position of the bands observed in the pictures, and the position of the periodic wavelength variation do not seem to correlate. I will further discuss these phenomena in the Discussion section.

---

*in the picture. This corresponds, with proper scaling to L_o = 2.25' (T_o = 0.66 sec.) in the lagoon.

A Note about Accuracy

A number of parameters influence the accuracy of surface flow measurements from wave data. The most obvious ones are the following:

1. Aberration in the optical system of the aerial camera.
2. Aerial camera deviation from verticality.
3. Accuracy of wave imaging by specularly reflected sunlight.
4. Accuracy of direction and scale references used during processing.
5. Resolution of the 2D Fourier transform processing.
6. Accuracy of calibration of the 2D Fourier transforming setup.
7. Accuracy of graphic determination of the flow from the 2D Fourier transform of the aerial photo.

In all of these parameters very good accuracy, of two percent or better in wavelength, can be achieved fairly easily, except on the resolution of the 2D Fourier transform, and I will explain why. Good aerial cameras are easily obtainable, and lens aberration should not be a factor in picture accuracy. The verticality of aerial photo, or insuring that the plane of the film will be horizontal, can be achieved high degree of accuracy; it depends on the pilot photographer team-work and on having a good mount for the camera. Aerial photos taken at an oblique angle also can be rectified when the angle is known. In a few of the data pictures I used, railroad rails are evident. The image distance between the rails did not vary (to the accuracy of my measurement) between the center and the edges of the photographs, in a couple of photos that I checked, showing both good horizontal control

of the photograph, and distortion free imaging. The Appendix shows how waves can be imaged with high accuracy, by specularly reflected sunlight.

The direction and scale references can be incorporated with high accuracy by careful planning of the measurement and processing of the data. I used the horizontal distance between two electric poles, and the direction of a level line in a parking lot, that I measured, as a basis for my references. After repeated measurements of the distance between the wave generators on different data slides, I found it to be within about 1% of a particular value. This includes any inaccuracies due to the aerial photography as well as the scale references. As a result, I expect my distance measurements on the data slides to have an accuracy of about 3%. The accuracy of the flow speed in the direction of the waves is roughly 25% lower than that of the distance measurement (see equation 11, page 46) and thus would be about 4% if no other factors were involved. Repeated determination of flow direction in the data made it apparent that they all were within 5°.

The resolution of the 2D Fourier transformer depends on the type of flow that is measured. The resolution of this transformer (see chapter on data processing, equation 13) is proportional to $\frac{d}{a}$. a is the diameter of the area being processed, and d is the wavelength of the waves in that area. Thus the larger the area being processed, the more accurate is the determination of the wavelength of the waves inside that area. When the wavelength of the wave train varies within the area that is being processed, such as when the flow is changing in that area, the resolution will be reduced. The bright spots in the

Fourier transforms will increase in size, or multiple spots will appear. When I started to process the data I used an aperture that contained about 25 waves. This should offer a resolution that is better than 4% in wavelength (5% in flow speed), for a homogeneous flow. I found that some Fourier transforms showed multiple waves from each wave generator, spanning about 25° in direction. I reduced the area being processed to approximately 10 waves, and the multiplicity of waves disappeared. This reduced the theoretical resolution to 10% in wavelength (about 12.5% in flow speed), but increased the actual resolution. The theoretical resolution is very conservative when applied to the wavelength measurement of one wave train, as it involves determining the center of a bright spot. Therefore I expect the accuracy of my wavelength measurements to be better than 5% on the average, which is reflected by about 6-7% accuracy in the determination of the flow speed component. The calibration accuracy of the 2D Fourier transformer is very good, and did not introduce any observable errors.

In summary, the accuracy of the method to determine the flow speed in the direction of the waves depends mainly on two factors; one is the scale references in determining distances in the data slides that brings a scatter of about 4% in the flow data; the other is the variability of the wavelength, due to the spatial variability of the flow or other reasons, which accounts for an approximately 7% scatter in the resulting flow values for this experiment. These values assume first class aerial photography that include suitable equipment (e.g. airplane, camera), and capable operators. In practice, I expect about twice the r.m.s. of the values calculated above,

or the measured flow component velocity values to be within 16% of the actual values for vertically homogeneous flows.

Another source of potential error is "stray" coherent wave sets that may rarely appear in the region being observed. The following example will illustrate the point.

Two Fourier transforms of a region in the lagoon gave results that were highly inconsistent with the other results. One of the wave sets in those transforms seemed to be in an unexpected direction; its wavelength was within reason. If it were a wavetrain produced by one of the wave generators, and reflected from the other shore of the lagoon, the flow measurement should have been correct, when using this wavetrain to calculate one component of the flow. This is due to the theoretical result derived in the chapter on Waves and Flow, that knowledge of the "history" of propagation of the waves is not required; all that is needed to determine the flow is their period. Such a reflected wave would have had the right period. A look at the original aerial photo solved the mystery. In the region of the lagoon from where these inconsistent transforms were obtained, a coherent "stray" wave train was observed arriving from the lagoon's northern entrance. Also, at that region, the wave train generated by one of the wave generators was not visible in the aerial photo. Such "stray" coherent waves with approximately, but not exactly, the "right" wavelength probably are highly unusual. But when they do occur, the original aerial photo will point them out.

The case of a vertically inhomogeneous flow has been treated in the chapter on Waves and Flow. For a flow monotonically and

slowly decreasing with depth, the wave data will result in a flow value that corresponds to the flow at a depth of $\frac{L}{12}$, fairly close to the surface. An idealized layer type flow has to be about that close to the surface to be noticeable by the waves (see equation (10) and Table 1). When measuring a real layer type flow, where the maximum flow speed occurs at a certain depth, the wave method will obviously indicate flow values below the maximum flow speed. These measured flow values will be larger, however, than ones obtained from an idealized layer flow model with parameters corresdponding to the real flow. This is further

analyzed in the discussion section. In principle, the profile of the vertical shear can be determined by using probing coherent wavetrains with different periods. The value of the flow would then be found for each period, or wavelength, in the way used in this thesis, assuming the flow to be homogeneous. This would supply a set of values $C-C_1$ as a function of k, and with the aid of equation (8), the value of $U(z)$ can be found. Equations (8) and (10) apply to waves codirectional with the flow. Utilizing them for oblique incidence would require some modification. In practice, when measuring flows in deep water, measuring the flow with coherent waves of more than one frequency allows one to tell whether the flow is vertically homogeneous, and if not, what sort of vertical shear exists.

As discussed above, the accuracy of the flow measurement depends on the nature of the flow. For vertically homogeneous flows, the flow speed should be measured with accuracy of better than 20%. For vertically inhomogeneous flows, the accuracy of the flow speed measurement may not be as good, unless a number of waves with different periods are used to probe the flow. Horizontally inhomogeneous flows can be measured with accuracy that is close to that of the homogeneous flow, if enough care is given to the averaging required in the processing, similar to that for the data in Fig. 21.

Discussion

In this thesis, I intended to develop a novel, remote and synoptic surface flow measuring technique, and tests its viability under "ideal" conditions; among other things I discovered that "ideal" conditions are difficult, if not impossible, to find. The data I

obtained from pictures of the waves gave evidence for some water motion that I did not expect, in addition to the mean flow, all of which was corroborated by current meter data. This emphasizes the capability of the wave method in determining surface flows.

Already during the initial experiments, conducted in a wavetank, the problem of obtaining an homogeneous flow for oblique incidence of waves was the most difficult. This was reflected by the scatter in flow measurements. Nevertheless, the flow component measured by waves agreed with flow determination by small floats. The next set of experiments were carried out in a natural body of water, Agua Hedionda, in Carlsbad, Ca. I obtained data in January and June 1979, as described in the respective chapters. Following is a discussion of the June data.

The data obtained in June 19, 1979 is shown in Figs. 17, 18 and 19. The flow, as determined by the wave data, is consistently lower than the readings obtained from the respective current meters, that were deployed at a depth of about 65 cm. The direction of the flow determined by both the current meters and the wave data (at the current meter position) is very close in value, and it follows a similar pattern of variation (with temporal scale of about four minutes) with time.

One feature of the flow obtained from both the current meters and wave data, is the variability of the flow measured by them, both in time and space. The spatial "wavelength" of this variability in the wavetrain is very roughly 15 meters, while its temporal period is below a minute. This is evident in Figs. 17, 18, 19 and 20.

Comparison of flow values

First I will address myself to the difference in flow speed as obtained from the wave data and current meters. The current meters were deployed at a depth of about 65 cm (it is difficult to have this kind of meter any closer to the surface). The probing waves we generated had a wave length of 90 cm, and they would not "feel the bottom" if it were 65 cm deep. It is plausible that the flow was not homogeneous, and spot data that I have gathered by a hand-held bongo type flow meter (from an anchored boat in the lagoon) supports that. The flow meter is not very accurate, but the relative flow values are correct. Some of these measurements are listed in Table 3.

	Measurement #			
Depth	1	2	3	4
6"			below calibration range*	
1'	10-11	26	10	below calibration range*
2'	10-11	32,24,30	10	8.5 - 9.5
3'	5 or less			

*If calibration curve were extended, it would read 5 cm/sec.

Table 3

Measurements by hand-held bongo type flow meter values in cm/sec

The data in Table 3 suggests the possibility that the flow was weak near the surface and assumed its full speed below 6" depth. In the chapter "Waves in a Flow" I have looked into the effect of a layer

type flow below the surface on the propagation of waves above. According to the model used there, the phase speed of 1 m waves will be modified by $.3\,U_o$ due to a codirectional Gaussian-like layer flow, with maximum U_o at depth of 10 cm and layer thickness of the order of one meter. Correspondingly, the flow measurement by the wave method will indicate a flow value that is smaller than the maximum speed of the flow, U_o.

If the discrepancy between the flow measurements with current meter and wave data is due to a layer flow below 6", the model predicts (by equation 10 and Table 1) a much larger discrepancy than the one observed. This can be attributed to the following: the layer model is based on the linearized equations of motion, assuming negligible wave amplitude, and thus, negligible water velodity. In the experiment, the observable waves had finite amplitude, and their troughs were close to the depth of the top of the layer, thus rendering the model somewhat conservative in its prediction on the effect of the layer flow on the wave speed. To summarize, there is evidence, from the measurements presented in Table 3 and the layer type flow model coupled with the discussion above, that the consistent lower flow speed values from wave data, as compared to current meter data, are due to a layer type flow below the surface. The good corroboration in the determination of flow direction for both measuring methods implies that they both measured the same flow at different depths; any errors (noise) in the determination of one or both flow components by the wave method, would have resulted in significant fluctuations in the flow direction values, when compared to the current meter data.

The above suggests that coherent wave trains in two or more frequencies and direction will be helpful in finding out the vertical profile of the flow.

Flow variability

The variability of the flow that I found from both the current meters and wave data suggests that there is more to the dynamics of the lagoon than the homogeneous steady flow, desirable for testing theories. Another flow measurement, carried out with a propeller type current meter (Cup type KAHLSICO #232 WA080) deployed close to the surface (about 1 m deep) at one position, gives more evidence for the temporal variability of the flow and its magnitude. This measurement, described in Table 4, shows the variability diminishing towards the afternoon (low tide was at 3:31 p.m.).

1:45-1:49 p.m.	10.7	cm/sec	2:33 p.m.	15.5 cm/sec
	13.5	"		
	19.3	"	2:40 p.m.	15.4 "
	15.4	"	2:41 p.m.	14.6 "
1:50 p.m.	12.25	"	2:57 p.m.	14 "
	18	"	2:58 p.m.	18 "
			2:59 p.m.	18 "
1:53 p.m.	17.5	"		
1:54 p.m.	13.1	"	3:31 p.m.	14.6 "
			3:32 p.m.	15 "
1:59 p.m.	16.2	"	3:33 p.m.	13.5 "
			3:35 p.m.	13.5 "

Table 4

Successive sampling of the surface flow averaged over 40 seconds, with a moored cup type current meter at about 1 m depth

Some of the sources for flow variability in the lagoon can be expected. In addition to turbulence due to the mean flow, there may be seiching in the lagoon, as well as motions induced by the ocean swell impinging on the lagoon entrance.

The period of the fundamental seiching mode in the lagoon, taking its approximate 900 m length and 5 m depth into account, is about 4 minutes. This period will be smaller during high tide, and larger at low tide. Evidence for this motion is seen in tide gage reading taken at the power plant water intake, shown in Fig. 23. Superimposed on the tidal variation is a water level oscillation of one-tenth to three-tenth feet height, with a period that is lower at low tide, and on the average is near 4 minutes. There are also about 4 peaks that can be seen in the data between 2 to 5 p.m., about an hour apart; their origin is unknown to me. Seiching along the approximately 300 m width of the lagoon should have a period of about 90 seconds. I have visually observed from shore, by the wave generators, water level variations with a period of somewhat more than one minute.

Some of the "action" in the lagoon can be seen in Fig. 24. Waves can be observed propagating from the northern entrance of the lagoon. A meandering flow may also be evident. The difference in scale between the waves produced by the wave generators and natural water motions is striking. Yet when properly observed, the artificial waves tell an informative story.

The variety of water motions in the lagoon explain some of the scatter in the data. Such waves and flows sometimes require averaging of the data over a judiciously chosen region, depending on the scale of flow that is of interest. An example of such averaging was performed on the data from Jan. 19, 1979 (see section on data processing for optical averaging).

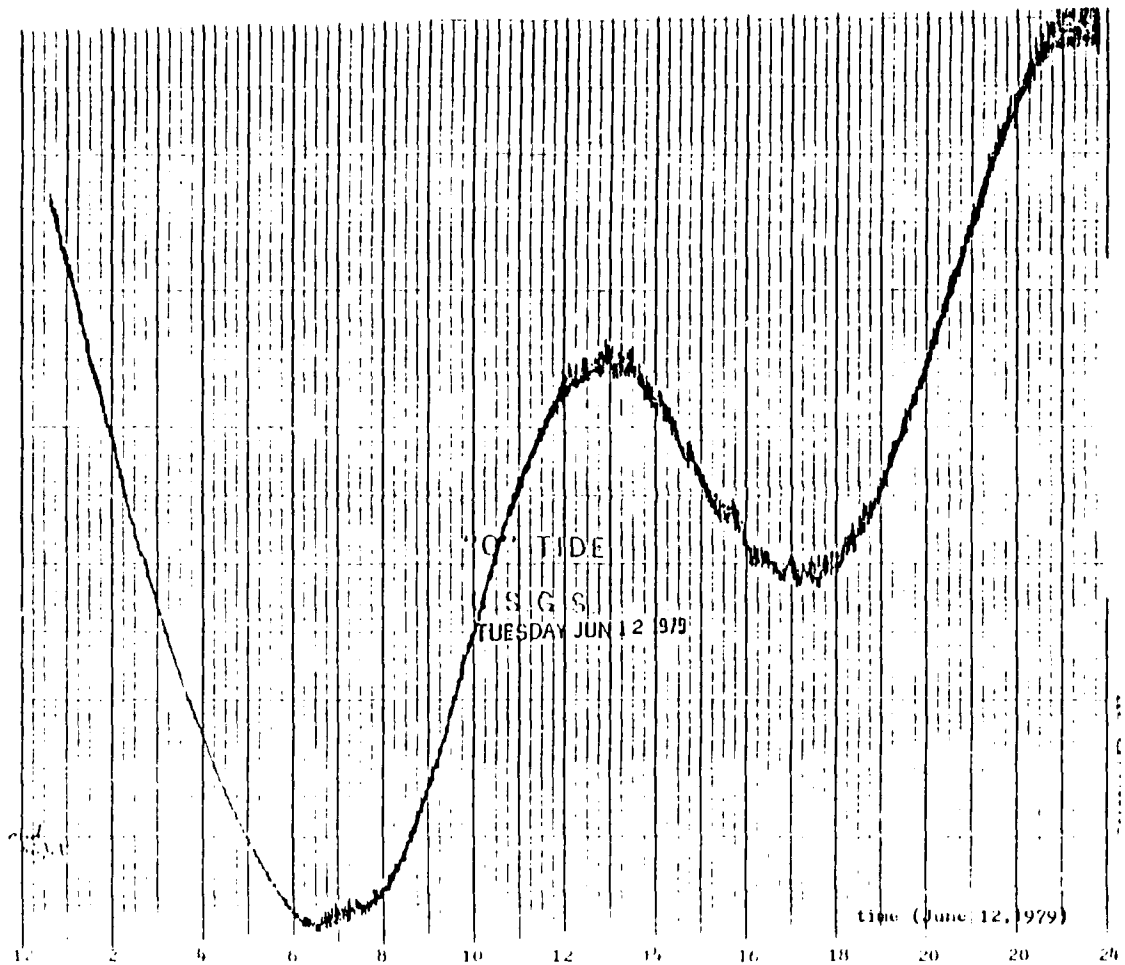

Figure 23. Tidal gage readings taken at the power plant water intake.

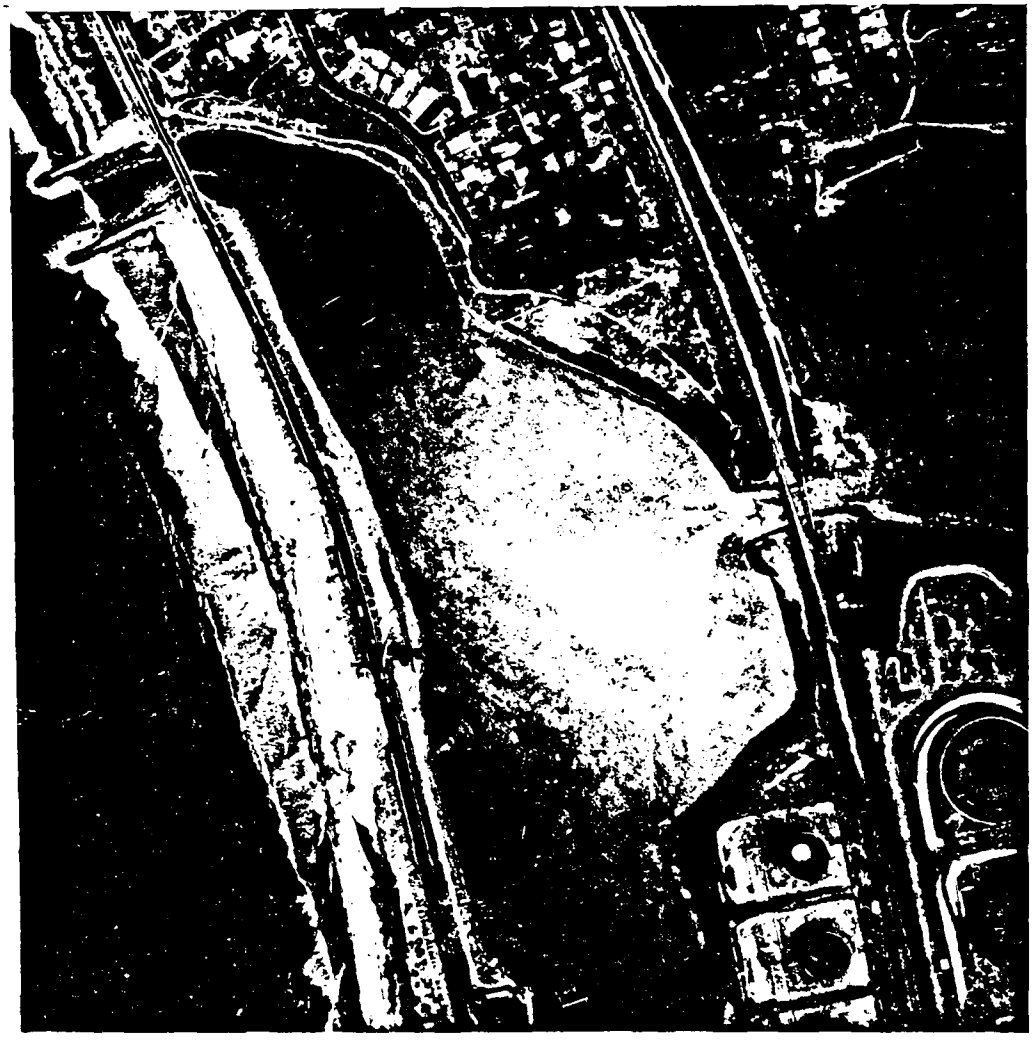

Figure 24.

Specular reflection of sun light from the lagoon surface.

Figure 21, that is an aerial photograph of the waves taken on January 19, 1979, shows period "banding" of the waves. These bands are located along the crests of the waves, rather than along any other geometrical feature; it is thus reasonable to assume that they originate in the wave paddle. The periodic wavelength variations, shown in Fig. 22, do not correlate in their location with the position of the "bands". These "bands" seem to be a variation of wave visibility, and thus could be a variation in wave slopes. The "bands" are about 12 waves apart. The period of the waves is .66 sec; assuming the "bands" were generated by changes at the wave generator, they were generated every $.66 \cdot 12 = 7.9$ seconds. All the above suggests that these "bands" are the result of lagoon water level variation due to 8 sec. ocean swell appearing at its entrance.* The wavelength variations with a spatial period of about 30 waves (see Fig. 22) is probably one of the several motions in the lagoon's water. The origins of the latter are not clear but they may be the result of interactions between the flows and waves discussed above, and perhaps their further interaction with the beach. The study of the dynamics of the lagoon is out of the scope of this thesis, although it is in itself an interesting subject. The synoptic measuring technique developed in this thesis could be used well as a tool for such a study.

Modulation of both wavelength and wave slope contain useful

---

*Ocean wave data obtained that day in Oceanside, Ca., courtesy of the California Coastal Engineering Data Network, Institute of Marine Resources, indicated wave energy having a frequency band that peaked near 0.125 cps (T = 8 sec.). Oceanside is located about 2 miles north of the Agua Hedionda lagoon.

AD-A110 957 SCRIPPS INSTITUTION OF OCEANOGRAPHY LA JOLLA CALIF I--ETC F/G 20/4
REMOTE SYNOPTIC SURFACE FLOW MEASUREMENTS IN SMALL BODIES OF WA--ETC(U)
SEP 80 D SHERES, J D ISAACS N00014-76-C-1103

UNCLASSIFIED NL

2 OF 2
AD A
110957

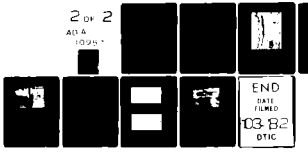

information which is utilized by this flow measuring technique to bring out different flow characteristics that may be difficult, if not impossible, to obtain by any other flow measuring technique. The temporal variation of the flow is also obtained by successive aerial photos of the same region, as was done in the experiment described in this thesis.

Potential application to the open ocean

It is certainly of interest, indeed very challenging, to apply this remote and synoptic flow measuring technique to the open ocean. The fact that the lagoon had a complicated flow system will be helpful in planning any flow measurements in the highly complicated flows of the ocean. Finding sources of coherent waves with known period in the open ocean is another problem for ocean measurements.

One solution could be utilizing boat waves; moving boats leave a signature of coherent wave trains, that is visible from the air over relatively large distances. The wave train following a boat propagates with a phase velocity that equals the boats' velocity; both velocities are with respect to the water that the boat is sailing through. Boat waves by themselves can supply information on the lateral variation of the surface flow over the region illuminated by the waves. To obtain absolute values of the flow (with respect to a stationary observer) requires additional reference data; the boats' velocity with respect to a stationary reference, or a surface flow value obtained independently at a point "illuminated" by the waves, comprise such data. Data about boat speed with respect to a stationary reference can be easily obtained in harbors, bays and

coastal waters, without the cooperation of a boat operator. One way to obtain such data is by successively timed aerial photographs of the boat, that include a number of stationary reference points on shore. Clearly any drifting object, like a drogue, can supply flow velocity data along the path of the drifter. However, the waves produced by the boat have the potential of supplying synoptic flow data over the area "illuminated" by the boats' waves.

In order to obtain some preliminary entree into the measurement and utilization of boat waves, I proceeded with a simple test in the Agua Hedionda lagoon, employing a small inflatable boat. The boat moved across the lagoon at constant throttle position. Vertical aerial photos were taken of the boat and its waves every 5 seconds. By comparing the successive position of the boat with reference points on shore, the speed of the boat, with respect to solid earth, was determined. The speed of the boat with respect to the water mass it was in, was determined from the wavelength of the waves following the boat with the boat's speed. I assumed that the water mass had a spatially uniform velocity. The difference between the speed values of the two methods is the flow velocity in the direction of the boat. Figure 25 shows the boat and the waves it produced. Table 5 shows the data collected. The accuracy of boat speed measurements here was only fair, as the airplane made some sharp turns in order to stay with the boat.

Figure 25.

Waves produced by a moving boat.

Time	Cb Boat speed w/r to "solid earth"	Cw Wave speed	Cw-Cb
	Boat crossing towards the northwest		
11:18 a.m.	2.065 m/sec	2.86 m/sec	.8 m/sec
11:19 a.m.	2.01 m/sec	2.76 m/sec	.75 m/sec
11:35 a.m.	3.33 m/sec	3.06 m/sec	-.27 m/sec
	Boat crossing towards the southeast		
11:13 a.m.	3.25 m/sec	2.7 m/sec	-.55 m/sec
11:24 a.m.	4.11 m/sec	3.2 m/sec	-. 9 m/sec

Table 5

Boat speed compared to the speed of the waves it generated

There were no current meters in the region where the boat was moving. From familiarity with the circulation pattern of that lagoon the approximate flow direction that is deduced from these pictures is reasonable.

These preliminary results suggest that meaningful remote and synoptic surface flow measurements can probably be carried out by observation of moving boats and the waves they produce. This could be especially useful for flow measurements in inaccessible harbors, bays and coastal waters. The cooperation of boat operators is not required for such measurements.

The application of boat waves to flow measurements will certainly require more research work, including a good understanding of the spectrum of the various waves generated by boats. Figure 9 shows a set of boat waves in the ocean which are certainly visible and coherent in the complicated nearshore ocean environment.

Conclusion

The research done for this thesis has been quite involved, carrying a new idea of remote and synoptic surface flow measurement from its conceptual "birth" through the theory and the development and construction of the various experimental and data processing equipment. Experiments conducted both in a wave tank and in the Agua Hedionda lagoon (in Carlsbad, Ca.), have demonstrated the viability and utility of this flow measuring technique for small bodies of water, such as harbors and bays. The equipment used was simple, cheap and readily available. No basic problems with this flow measurement technique have surfaced during the experiments, both in the wave tank and in the lagoon.

This thesis also outlines how to conduct such flow measurements, and how to utilize the simple and powerful 2D Fourier transform in analyzing the data. Utilization of available image processing hardware and software can speed up the process of surface flow calculation from the aerial pictures.

Any extension of this work to the open ocean should not confine itself to use this approach in its "pure" form. Any available clues on the flow, such as total reflection of waves, breaking waves, a current meter in a strategic location, etc., should be incorporated in the measurement. A picture of the specularly reflecting ocean surface can supply a lot of information when properly interpreted, and it shcuild be used.

References

Barber, N. F. 1954. Finding the direction of travel of waves. Nature 154: 1048-1049.

Biesel, F. 1950. Etude theorique de la houle en eau courante. La Houille Blanche, 5, No. special A, 279-285.

Dalrymple, R. A. 1973. Water wave models and wave forces with shear currents. Coastal and Oceanographic Engrg. Lab., University of Florida Technical Report No. 20.

Cox, C. S. and W. H. Munk. 1954. Statistics of the sea surface derived from sun glitter. J. Marine Res. 13: 198-227.

Evans, M. W. and T. M. Georges. 1979. Coastal Ocean Dynamics Radar (Codar): NOAA's Surface Current Mapping System. Oceans '79 conference, San Diego, CA., September 17-17, 1979. IEEE publication number 79 CH 1478-7 OEC.

Goodman, J. W. 1968. Introduction to Fourier Optics. McGraw Hill Book Co., 287 pp.

Herbich, J. B. and L. Hales. 1972. The effect of tidal inlet currents on the characteristics and energy propagation of ocean waves. Fourth annual offshore technology conference, Houston, Texas, May 1-3, 1972. OTC paper No. 1618.

Huang, N. E., D. T. Chen, C. Tung and J. R. Smith. 1972. Interaction between steady, non-uniform currents and gravity waves with applications for current measurements. Journal of Physical Oceanography 2: 420-431.

Hulbert, E. O. 1934. The polarization of light at sea. J. Optical Soc. Am. 24: 35.

Ichiye, T. and Y. Sugimori. 1974. Holographic method of wave spectrum measurement. Proceedings of the international symposium on Ocean Wave Measurement and Analysis, New Orleans, LA., September 9-11, 1974.

Isaacs, J. D. 1948. Discussion of "refraction of surface waves by currents" by J. W. Johnson. Transactions, American Geophysical Union, Vol. 29 No. 5: 739-742.

Johnson, J. W. 1947. The refraction of surface waves by currents. Transactions, American Geophysical Union, 28(6): 867-874.

Kenyon, K. E. 1971. Wave refraction in ocean currents. Deep Sea Res. 18: 1023-1034.

Kipling, R. 1893. The Merchantmen.

Longuet-Higgins, M. S. and R. W. Stewart. 1961. The changes in amplitude of short gravity waves on steady non uniform currents. J. Fluid Mech. 10: 529-549.

Preisendorfer, R. W. 1976. Hydrologic Optics, Vol. 6. U.S. Dept. of Commerce, National Oceanic & Atmospheric Admin., 390 pp.

Schumann, E. H. 1975. High waves in the Agulhas Current. S. African Shipping News and Fishing Industry Review 30(3): 25-27.

Sugimori, Y. 1973. Dispersion of the directional spectrum of short gravity waves in the Kuroshio Current. Deep-Sea Research 20: 747-756.

Sugimori, Y. 1975. A study of the application of the holographic method to the determination of the directional spectrum of ocean waves. Deep-Sea Research 22: 339-350.

Stilwell, D., Jr. and R. O. Pilon. 1974. Directional spectra of surface waves from photographs. J. of Geophysical Research 79(9): 1277-1284.

Stewart, R. H. and J. W. Joy. 1974. HF radio measurements of surface currents. Deep-Sea Research 21: 1039-1049.

Unna, P. J. H. 1942. Waves and tidal streams. Nature 149: 219-220.

Whitham, G. B. 1974. Linear and Nonlinear Waves, chapter 11 and 12. John Wiley and Sons, 636 pp.

Wiegel, R. L. 1964. Oceanographic Engineering. Prentice Hall, Inc., Englewood Cliffs, N.J. 532 pp.

Wu, J. 1977. Effects of long waves on wind boundary layer and on ripple slope statistics. J. Geophys. Res., 82(9): 1359-1362.

APPENDIX

REMOTE AND SYNOPTIC WATER WAVE MEASUREMENTS BY AERIAL PHOTOGRAPHY
A MODEL, EXPERIMENTAL RESULTS AND AN APPLICATION

David Sheres
University of California
Scripps Institution of Oceanography and
Foundation for Ocean Research
La Jolla, California 92093

Abstract

This paper briefly reviews the parameters involved in aerial photography of coherent trains of surface waves. This includes the effects of water reflectance, waves, and sun and cloud conditions, on the quality of wave imaging in aerial photos. It also describes an analytical model of the specular reflection of sunlight by surface waves, together with experimental results from an outdoor wave facility. Analytical expressions are derived for the accuracy of wave-length measurements using aerial photos of waves. Further, it treats wave slope determination from aerial photos of ideal waves and presents experimental results from an outdoor wave facility.

The application of remote synoptic surface flow determination by imaging of surface waves is briefly discussed.

Introduction

Surface waves reflect light to an observer or camera. The slope and position of the waves and the position of the observer determine which part of the brightness source, such as the sky, cloud cover and sometimes shore, is reflected to the observer. When different parts of the waves reflect differing brightness to the observer, the waves become visible. The parameters involved are the spatial variation of the source brightness, and the reflection angle of the light from the water surface. The reflectivity of water is almost constant at reflection angles of 0-50 degrees, thus in a homogenously overcast or foggy day, when the light reaching the observer is reflected by the waves at an angle less than 50 degrees, the waves are not visible. Figure 1A, taken from Scripps pier early in an overcast morning, is an example of this case. Figure 1B was taken a few hours later when the sun was out. Steep waves are visible to an observer on a cliff near shore under most day-light conditions, as each wave reflects light from the cliffs as well as from the sky. Obviously there is a filtering effect by optical imaging of waves. In analyzing photographs of the water surface for their wave content, the effect of the parameters mentioned above have to be taken into account. Some waves may not show up in the pictures.

The water surface is covered by waves; gravity waves with maximum steepness of .142 (Wiegel Ch. 2.6) and maximum crest angle of 120 degrees. This means that when a wave of 120° crest angle passes below an observer, the wave scans the sky $\pm 60°$ (total of 120°) and reflects that sky light toward the observer. The wind-generated capillary waves are superposed on the longer gravity waves. The slope distribution of the ocean surface was measured at sea by Cox and Munk (1954) and found to have a Gaussian distribution with close to zero mean. The root mean square slope for a 20-knot wind (10 m/sec) was measured to be about 10°. The mean square slope was also found to be proportional to the wind speed. These results were recently verified by Wu (1977) in the laboratory.

Aerial photos of surface gravity waves in various bodies of water are now routinely obtained. We would like to gain as much information as possible on the observed wave parameters from these photos. This wave information can tell us about pertinent processes, such as directional wave spectra, sedimentation rates, and surface flow. In the following section I will analyze a model of specular reflection of sun light by coherent sinusoidal wave trains. This model determines the specularly reflecting glitter pattern observed due to a coherent wave train, and the distribution of the glittering facets on each wave in that wave train. The glitter pattern derived here is similar to the grid pattern Cox and Munk (1954) used for determining the wave slope statistics in their aerial photos. The approach here is focused on obtaining data from coherent gravity wave trains for applications such as the determination of surface flow by monochromatic waves.

Model

Let us analyze an idealized model, assuming sinusoidal wave with amplitude A, (small slope linear approximation) specularly reflecting a wide beam of collimated sunlight. We would like to find the assembly of points (x_o, y_o, o), that reflects the sun rays into the camera. These points appear as glitter points in the aerial photograph.

This work was supported by the Office of Naval Research under contract number N00014-76-C-1103.

CH1478-7/79/0000-0614$00.75 © 1979 IEEE

We would also like to determine the wave phase, from where the specular reflection reaches the camera, on successive waves. Any phase variation represents an error in the wavelength determination, and we would like to establish its dependence on the geometry of the situation.

In the model:

$\bar{I}$ is the incident ray of sunlight,
$\bar{R}$ is the ray specularly reflected by the wave.
$\bar{n}$ is the normal to the wave at the reflecting site.

It is easy to show[1] that

$$\bar{R} = \bar{I} - 2(\bar{I} \cdot \bar{n})\,\bar{n} \qquad (1)$$

Let us fix the wave direction as being along the x axis (crests parallel to the y axis), and the position of the camera at (0, 0, H). See Fig. 2. The sun is at an angle θ away from the zenith, and the projection of its ray $\bar{I}$ on the water surface makes angle ϕ with the direction of the waves (the x direction).

The specularly reflecting wave surface is described by:

$$Z = A \sin kx$$

A - wave amplitude
k - wave number
L - wave length $\qquad k = \frac{2\pi}{L}$
kx - the wave phase in radians.

The incidence wave is

$$\bar{I} = \tan\theta \cos\phi\,\bar{i} + \tan\theta \sin\phi\,\bar{j} - \bar{k} \qquad (2)$$

($\bar{i}$, $\bar{j}$, $\bar{k}$ are unit vectors along the coordinate axis) and the normal to the wave at a glitter point (x_o, y_o) is:

$$\bar{n} = (1 + A^2 k^2 \cos^2 kx_o)^{-\frac{1}{2}} \times (-Ak \cos kx_o\,\bar{i} + \bar{k})$$

For non-breaking waves $A^2k^2 < 1/10$ and we will approximate

$$\bar{n} = -Ak \cos kx_o\,\bar{i} + \bar{k} \qquad (3)$$

From equations 1, 2, 3 we obtain

$$\bar{R} = (\tan\theta\cos\phi - 2A^2k^2 \cos^2 kx_o \times \tan\theta\cos\phi - 2Ak\cos kx_o)\,\bar{i} + (\tan\theta\sin\phi)\,\bar{j} + (1 + 2Ak\cos kx_o \times \tan\theta\cos\phi)\,\bar{k} \qquad (4)$$

or

$$\bar{R} = D\,\bar{i} + E\,\bar{j} + F\,\bar{k}$$

$\bar{R}$ has to reach the camera at point (0, 0, H) from point (x_o, y_o, z_o) and thus

$$\bar{R} = -x_o\,\bar{i} - y_o\,\bar{j} + (H - z_o)\,\bar{k} \approx -x_o\,\bar{i} - y_o\,\bar{j} + H\bar{k} \qquad (5)$$

From 4 and 5

$$\frac{-x_o}{D} = \frac{-y_o}{E} = \frac{H}{F} \qquad (6)$$

or:

$$\frac{x_o}{D} = \frac{y_o}{E} \qquad (7)$$

$$\frac{y_o}{E} = \frac{-H}{F} \qquad (8)$$

$$\frac{x_o}{D} = \frac{-H}{F} \qquad (9)$$

Let us define

$$r = \tan\theta\cos\phi$$

$$q = \tan\theta\sin\phi$$

$$\eta = Ak\cos kx_o$$

From 7:

$$r - 2\eta^2 \quad r - 2\eta = \frac{x_o}{y_o}\,q \quad \text{and}$$

$$\eta = (2r)^{-1}\left(-1 \pm \sqrt{1 - 2r\left(\frac{x_o}{y_o}\,q - r\right)}\right) \qquad (10)$$

---

[1] The component of $\bar{R}$ parallel to the surface is the same as in $\bar{I}$. The component of $\bar{R}$ perpendicular to the surface has the same magnitude and opposite sense as that of $\bar{I}$.

From 8:

$$2\eta r + 1 = \frac{-H}{y_o} q \qquad \text{and}$$

$$\eta = \left(\frac{-H}{y_o} q - 1\right) \frac{1}{2r} \tag{11}$$

From 9:

$$\frac{-x_o}{H} (2\eta r + 1) = r - 2\eta^2 r - 2\eta \tag{12}$$

There are only two independent equations here, as is evident also in 7, 8, 9.

From equations 10 and 11, equating η, we obtain

$$y_o^2 (1 + 2r^2) - 2rqx_o y_o - H^2 q^2 = 0 \tag{13}$$

This equation has the form

$$y_o^2 - u\, x_o y_o - v = 0$$

$$u = \frac{\sin 2\phi}{1/\tan^2 \theta + 2\cos^2\phi}$$

$$v = \frac{H^2 \sin^2 \phi}{1/\tan^2 \theta + 2\cos^2\phi} \tag{14}$$

Eq.14 describes the locus of all points (x_o, y_o) that may specularly reflect into the camera. In order to find the points that can reflect sunlight into the camera, we have to check that the slopes required to achieve the reflections at these points (x_o, y_o) do not exceed the wave slope.

Equation 10 can be written as

$$\cos kx_o = \left(-1 \pm \sqrt{1 - 2r\left(\frac{x_o}{y_o} q - r\right)}\right) \times (2rAk)^{-1} \tag{15}$$

for $\cos kx_o = 0$ we obtain

$$\frac{y_o}{x_o} = \tan \phi \tag{16}$$

Thus the intersection between the lines described by equations 14 and 16 will determine the region where the specular reflection comes from the wave troughs and crests (zero slope). This is the specular point when no waves are present.

For $\cos kx_o = \pm 1$ we obtain

$$\frac{x_o}{y_o} = \frac{1}{\tan \phi} \pm \frac{2Ak}{\tan\theta \sin\phi} \cdot \frac{2 (Ak)^2}{\tan \phi} \tag{17}$$

The intersections of the lines described by equation 17 and the line in equation 14 are the points where maximum wave slope is required in order to specularly reflect sunlight into the camera. The waves are not visible further away (in this ideal model) from the specular point. The evaluation of wave slope from dimensions of specular regions has been approached before (Hulburt 1934, Cox and Munk 1954, Preisendorfer 1976) for random seas. Wave slope estimate is obtained here directly for coherent wave trains utilizing expressions developed above. Equation 17 gives an estimate of the wave slope, when the position (x_o, y_o), where the specular reflection of the wavetrain disappears, is used. A wavetank test for slope estimation is presented in the section describing experimental work. The word estimate is used, as this is an idealized model. This model can act as a basis for amplitude determination, when some other factors, such as distribution of capillary waves for particular wind conditions, are taken into account, as discussed at the end of this paper.

An example of the calculations above is presented in Figure 3, for the conditions $\theta = 45°$ $\phi = 45°$ $H = 1000$m. The curve represented by equation 14 is intersected by the two lines from equation 17, and the region representing the specularly visible wave train is drawn by a heavy line. The presentation of equation 14 consists of two symmetrical curves. Only the curve that makes physical sense was drawn in Figure 3.

The Distribution of Glittering Facets On Each Wave

The distribution of glittering facets on successive waves is found by solving equation 12.

Neglecting the $(Ak)^2 \cos^2 kx_o$ terms will result in a simplified form:

$$\cos kx_o = \frac{r + x_o/H}{(1 - rx_o/H)\, 2\, Ak} \tag{18}$$

The solution to equation 18 represents the positions x_o of the specularly reflecting facets on successive waves. Figure 4 presents such a solution for the case $\phi=0$, $x_o << H$ and small θ. The accuracy of wavelength measurements from aerial photos depends on the position of the glittering wave facets on successive waves. The wavelength of a coherent wavetrain in such a photo is determined by, and proportional to, the normal distance between successive glittering rows. This measure is generally accurate, particularly if the

wavetrain is known to be monochromatic and the distance between the glittering rows is constant. Equation 18 describes the quantitative variations in wavelength measure due to the geometry of the measurements. This can become conceptually clear by observing the example in figure 4A: the slope of the line

$$\frac{x_o/H + \tan\theta}{2Ak}$$

including variation of wave amplitude, may introduce errors in the wavelength determination. Let us calculate this error. Equation 18 can be written as

$$\cos kx_o = g(x_o)$$

Δx is an approximation for the change in position of glittering facets on successive waves. It can be found from the equation

$$g(x_o + L) - g(x_o) \cong \cos k(x_o + \Delta x) - \cos kx_o$$

or

$$g(x_o + L) - g(x_o) \approx \frac{\partial g(x_o)}{\partial x} \times L =$$

$$\frac{L}{H(1 - rx_o/H)\ 2Ak}\left[\frac{(r + x_o/H)}{(1 - rx_o/H)} + 1\right] \quad (19)$$

An example, that pertains to the conditions in the experimental wave tank, illustrates the use of this formula.

Assume $\theta=41°$, $\phi=0$, $H=6m$, $L=0.24m$, $2A=0.01m$.

At the specular point, the glittering facets are on the crests and the troughs, hence $kx_o = \frac{\pi}{2}$ and $\cos kx_o=0$. From equation 18, $x_o = -H \tan\theta = -5.2m$. Hence by equation 19:

$$\frac{\partial g(x_o)}{\partial x} \times L = 0.09$$

At x_o, the specular point, the line g(x) intersects the sinusoid $\cos kx_o$ near the zero crossing. See figure 4 for a similar example. In that region

$\cos k(x_o + \Delta x) - \cos kx_o = 0.09$ corresponds to $\Delta kx = 5.2°$. $5.2/360=1.5\%$ change in wavelength.

A similar calculation for waves on the edges of the specular pattern, shows for this example a phase variation of $\Delta kx = 36°$ or 10% change in wavelength. For the wave just before the edges, $\Delta kx=16°$. the wavelength change is down to 4.5%. These variations are due to the small slope of the cosine term in equation 18, near the edges of the specular region. Figure 4A should again help in visualizing these results. In cases where the expected wavelength measuring errors predicted by equation 19, due to factors like amplitude variations or large wavelength waves, are not acceptable, an increase in camera height is a simple remedy.

Experimental Setup

An outdoor wave basin was used to test the viability of the above model. It includes an 8' X 30' wave basin, a beach, and a wave generator. The wave generator has an 8' paddle driven by a 1 H.P. synchronous motor through a 10:1 reducer. The motor receives its power from a variable frequency drive that maintains a preset frequency. On checking the motor RPM over periods of approximately an hour no frequency shifts were found.

The specular reflection of sunlight from the waves is recorded by a camera mounted on a platform above the wavebasin. Verticality of picture taking was maintained by a circular level attached to the camera back. The wave amplitude was measured by photographing a thin grid placed along the waves.

This setup enables wave measurements with $\phi=0$, or the sun rays' projection on the water surface parallel to the wave direction.

Experimental Results

The position of the specularly reflecting facets on the surface of waves is shown in figure 5. It represents $\phi=0$ and should be compared to figure 4B. The specular rows are equidistant at the center of this region (the specular point). The specular rows "organize themselves" into couples that get closer together the further away they are from the center. These couples coalesce before they disappear further away from the center. This distribution of specular points is intuitively obvious for the simple geometry of the example presented in figures 4 and 5. The specular points occupy positions of zero slope (crest and trough) at the center of the specular region, while further away from it they "move" in pairs towards the high slope zero crossing region of the waves.

The wavelength of the waves was measured by three vertical photos (similar to figure 5 but not shown here) of waves with period of 0.38 seconds, taken when the sun was at $\theta=41°$ from zenith. The camera was on a platform 6 meters above the wave tank. A reference length at the water surface, visible in the photograph, helped determine wavelength. From each photo I measured 20 wavelengths along a line parallel to the wave direction. The wavelength, averaged for 6 groups

of ten measurements each were:

24.3 cm (RMS=.96cm), 24 cm (RMS=.58cm), 24 cm (RMS=.91cm), 24.2 cm (RMS=1cm), 24.4 cm (RMS=1.22cm), 24.2 cm (RMS=.9cm). (RMS is the Root Mean Square).

The average wavelength is 24.18 cm. An independent direct wavelength measurement is presented in figure 7. A ½-inch grid is placed in the water, along the wave direction, two meters away from the wave generator. Two waves are observed along the grid. One has a wavelength 9.5" (24,13 cm), the other 9.75" (24.76 cm). The average is 24.4 cm. The doubt in reading the data is close to 1 cm. Thus the very good agreement of both wavelength measurements may be somewhat fortuitous.

The grid used for wavelength measurements in the water was also handy for amplitude measurements. As can be seen in Figure 7, the amplitude of the waves is 0.5/2 inches =0.63 cm ±10%. From the vertical pictures of the waves, when no wind effects were observed on the water, the glitter pattern disappeared at x_o = -2.7 meters ±0.3m. From equation 12, assuming $\eta^2 r < \eta$

$$\frac{x_o/H + \tan\theta}{(1 - x_o/H \tan\theta)\ 2Ak} = +1$$

with H=6m, tanθ=.87, L=0.24m,

gives A=0.58 cm.

The grid was about 2.5m away from x_o (where the glitter pattern disappeared) closer to the wave generator.

Discussion

The simple model discussed here offers some insight into the parameters involved in aerial photography of surface waves. Equations 10, 11, 12, can be used to determine what part of the wave is specularly reflecting at a particular geometry of illumination, waves, and camera. The accuracy of wavelength measurements from aerial photos is found by utilizing equation 19. The effect of wave amplitude changes on this accuracy can be similarly obtained. The effect of wind produced capillary waves that are superposed on the gravity waves, is clearly of interest. This extension of the present paper can be analyzed by a perturbation of slope of the sinusoidal waves presented here. Figure 6 is a picture of specular reflection of wind generated capillaries superposed on gravity waves. Their effect can be assessed by comparing figure 6 to figure 5, taken when not much capillary action was observed. The capillary waves tend to coalesce the specularly relecting row pairs on the high slope region of the gravity waves. This effect will not alter the wavelength measurement accuracy much, if at all. Amplitude estimation will certainly be influenced by the superposed capillaries, but in a predictable manner. The capillary waves will extend the specularly reflecting region, and therefore give an amplitude estimate for coherent gravity waves that is larger than it actually is; this "extra" amplitude can be assessed if the wind is known. On the other hand, the extension of the model presented here to include the capillary wave effects may help, if used in reverse, in assessing wind conditions from aerial photographs of known coherent wave trains.

The interest in wave data is many fold: on the one hand is the inherent interest in the directional spectra of waves and how they are going to influence the marine environment, activities, and the coast line. On the other hand, natural waves as well as artificially generated coherent wave trains can be used to extract information on the condition in various bodies of water. Both shoaling and surface currents do affect surface gravity waves; both can be determined by intelligent observation of coherent wave trains in the region of interest. Gravity waves of a fixed period exhibit a wavelength that depends on the surface flow that they propagate through. (Their period remains fixed with respect to a stationary observer). This ultimately enables surface flow determination from wavelength and direction measurements of two or more wavetrains with known frequency, propagating in different directions. These wave data can be readily and accurately collected by aerial photographs of the waves glitter pattern.

Acknowledgments

I thank John D. Isaacs for suggesting the subject of this research and for his helpful discussions; John Lyons for constructing the experimental facility; and the Office of Naval Research, Geography Section, for their support.

References

Cox, C.S., and W.H. Munk. 1954. Statistics of the sea surface derived from sun glitter. J. Marine Res., *13:* 198-227.

Hulburt, E.O. 1934. The polarization of light at sea. J. Optical Soc. Am., *24:* 35.

Preisendorfer, R.W. 1976. Hydrologic Optics, Vol. 6. U.S. Dept. Commerce, National Oceanic & Atmospheric Admin., 390 pp.

Wiegel, R.L. 1964. Oceanographical Engineering. Prentice Hall, Inc., Englewood Cliffs, New Jersey, 532 pp.

Wu, J. 1977. Effects of long waves on wind boundary layer and on ripple slope statistics. J. Geophys. Res., *82(9):* 1359-1362.

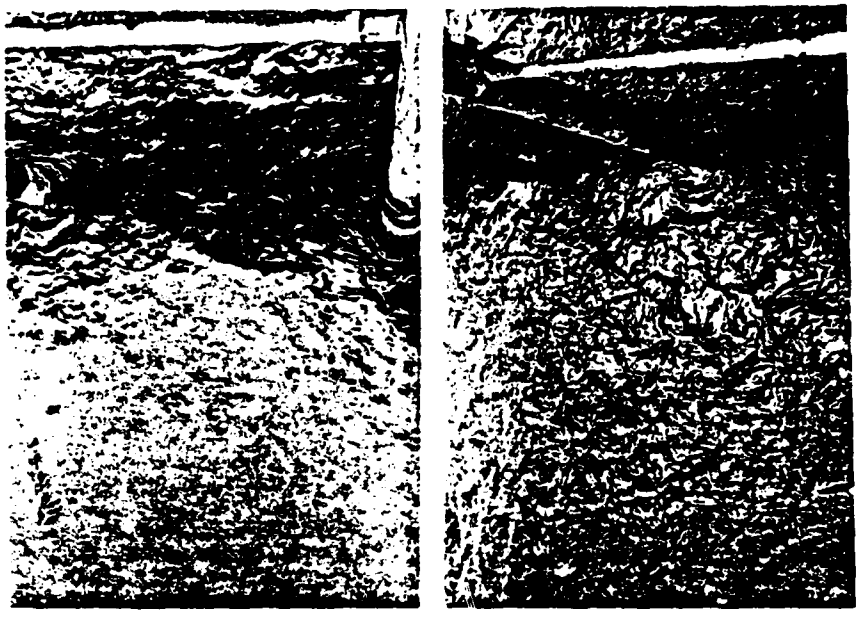

A. B.

Figure 1a. A. Water surface as viewed from Scripps pier on an overcast morning.
B. The water surface a few hours later after the sun came out.

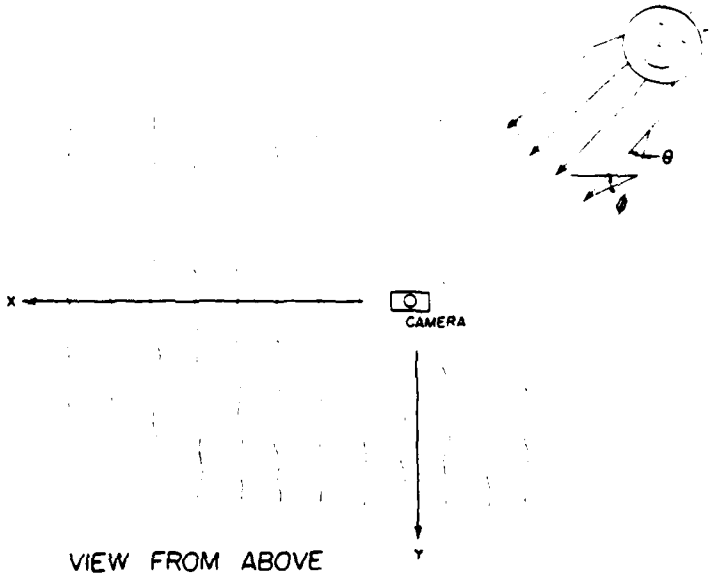

Figure 2 a. Model layout

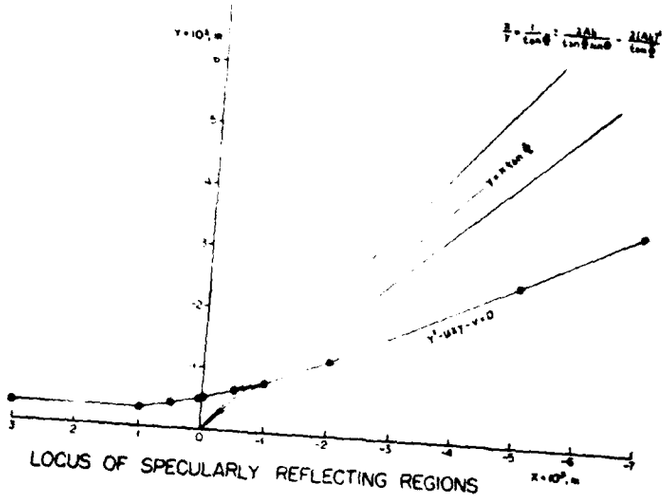

Figure 3a. Graphical determination of specularly reflecting wave positions for camera height of 1000 m. ϕ=45° , θ=45°.

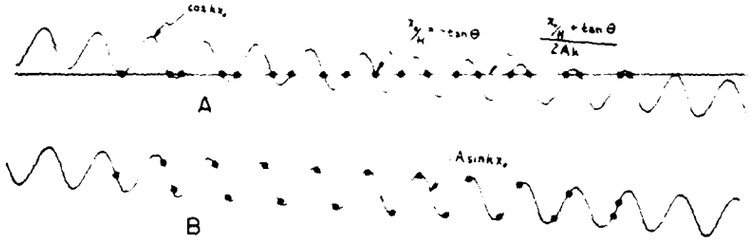

A. GRAPHICAL SOLUTION OF $\cos kx_o = \frac{z_{/H} + \tan\theta}{2Ak}$

B. SPECULAR REFLECTIONS ON THE WAVE

$Z = A\sin kx_o$

Figure 4a. Positions of specularly reflecting facets on the waves for ϕ=0, small θ, and $x_o < H$.

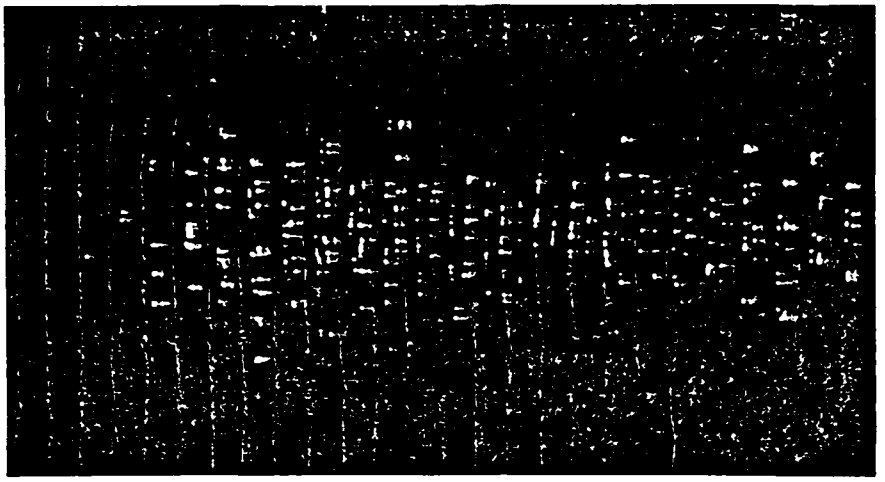

Figure 5a. Specular reflection of sun light by a coherent gravity wave train. The wind is negligible. The parallel bright lines covering the picture are due to focusing of sun light by the waves on the bottom of the wave pool.

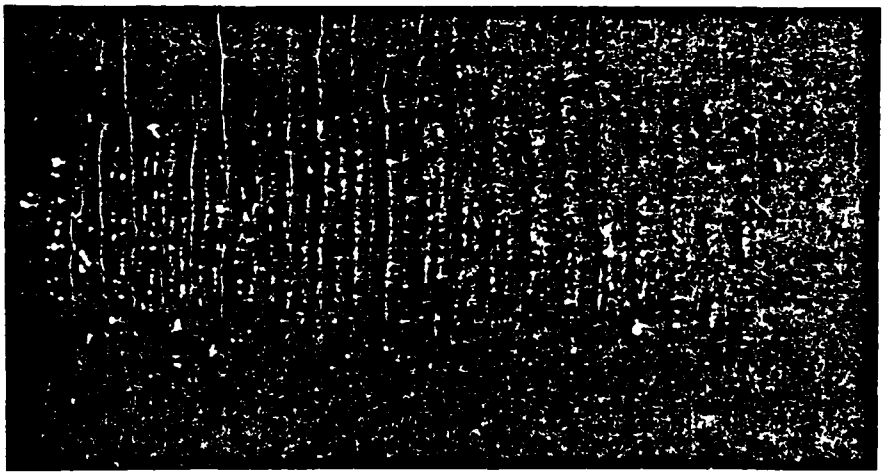

Figure 6a. Specular reflection of sun light by wind generated capillaries superposed on gravity waves. The parallel bright lines covering the picture are due to focusing of sun light by the waves on the bottom of the wave pool.

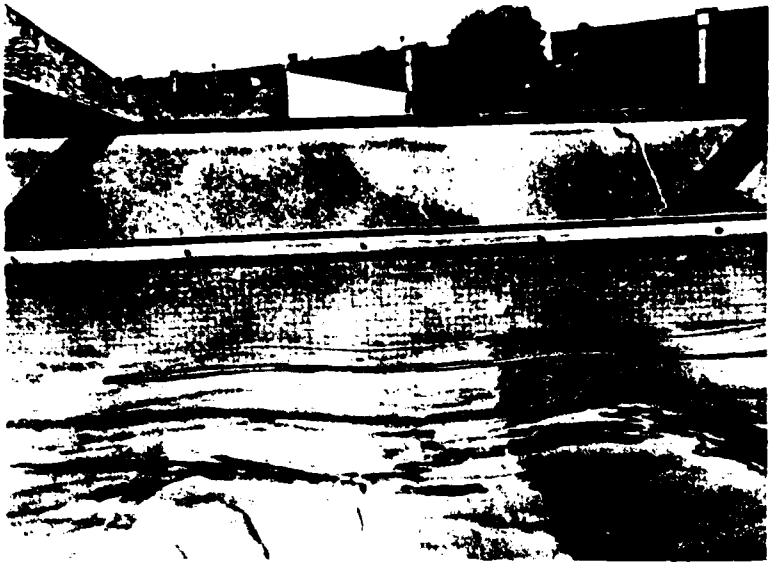

Figure 7a. Wave length and amplitude measurement by a ½-inch square grid placed in the waves.

END

DATE
FILMED

03-82

DTIC